



Multiple shear band development and related instabilities in granular materials

A. Gajo^a, D. Bigoni^{a,*}, D. Muir Wood^b

^a*Dipartimento di Ingegneria Meccanica e Strutturale, Università di Trento, Via Mesiano 77-38050 Povo, Trento, Italy*

^b*Department of Civil Engineering, University of Bristol, Bristol, UK*

Received 24 November 2003; received in revised form 4 May 2004; accepted 19 May 2004

Abstract

A new, small-strain constitutive model, incorporating elastoplastic coupling to describe developing elastic anisotropy, and density as a state variable to capture compaction and dilation, is proposed to simulate the behaviour of granular materials, in particular sand. This developing elastic anisotropy is related to grain reorientation and is shown to be crucial to obtain localisation during strain hardening, as experiments exhibit. Post-localisation analysis is also performed under simplification assumptions, which evinces a number of features, including softening induced by localisation, size effects and snap-back, all phenomena found in qualitative and quantitative agreement with experiments. No prior model of granular material deformation correctly captures *all* these behaviours.

The post-localisation analysis has revealed a new form of material instability in granular materials, consisting of a saturation mechanism, in which shear bands just formed unload, permitting new bands to form. This phenomenon shares similarities with the mechanics of phase transformation in metal strips and results in a stress oscillation during increasing deformation. The investigation of this mechanism of localised deformation reveals that loose and dense sands behave in qualitatively different ways. In particular, saturation is not persistent in dense sand; rather, after several shear bands form and saturate, this process is terminated by the formation of a differently inclined shear band occurring in the material transformed by previous strain localisation. In this case, the resulting ‘global’ stress–strain curve exhibits a few stress oscillations followed by a strong softening. On the other hand, band saturation is found to be a persistent

*Corresponding author. Tel.: +39-0461-882507; fax: +39-0461-882599.

E-mail addresses: gajo@ing.unitn.it (A. Gajo), bigoni@ing.unitn.it (D. Bigoni), d.muir-wood@bristol.ac.uk (D.M. Wood).

URL: <http://www.ing.unitn.it/~bigoni/>

phenomenon in loose sand, yielding a continuing stress oscillation. This provides a consistent description of specific experimental results.

© 2004 Elsevier Ltd. All rights reserved.

Keywords: Strain localisation; Post-critical analysis; Band saturation; Sand; Elastoplasticity

1. Introduction

Strain localisation is a common phenomenon in granular materials, which has been thoroughly analysed both from experimental (Vardoulakis and Graf, 1985; Han and Drescher, 1993; Tatsuoka et al., 1990; Finno et al., 1997) and theoretical points of view (Schaeffer, 1990; Schaeffer and Shearer, 1997; Shearer and Schaeffer, 1994; Vardoulakis, 1978).

From the experimental point of view, nucleation and growth of shear bands have been investigated under various testing conditions—for instance, a specific biaxial apparatus has been developed (Drescher et al., 1990)—and employing a number of sophisticated techniques, including stereophotogrammetry (Desrues et al., 1985; Finno et al., 1997), X-ray radiography (Roscoe et al., 1963; Roscoe, 1970) and X-ray tomography (Desrues et al., 1996), so that many aspects of the physics of shear bands can be assumed to be well-documented. This point will be important for our study, since we will systematically make use of information available from experimental evidence.

From the point of view of mechanical modelling, despite the large number of papers devoted to the topic, the situation still appears to be rather unsatisfactory. We suggest that shear band analysis should rely on a firm (physically well-motivated and accepted) constitutive framework, but this is not easy to obtain for granular media, for at least two reasons. First, even though constitutive modelling in soil mechanics has been studied for over 40 years, a generally-accepted constitutive model for a sufficiently broad class of soils is still lacking. Second, and more important, models on which a certain agreement has been reached, such as for instance the Cam–clay model, have been developed to capture homogeneous behaviour, without specific consideration of the modelling of instabilities. This is particularly true for local instabilities such as shear bands and surface phenomena. In other words, there are features of constitutive response and experimental setup that may be unimportant when the global response of a sample has to be described, but that become essential in analyses of bifurcation and instability. For example, it will be shown that induced elastic anisotropy is one of such features.

As a complement to the above discussion, we note that the introduction of specific numerical remedies to the ill-posedness of problems involving strain localisation has additionally complicated the situation, so that constitutive features have been added to the models (for example, non-locality or viscosity) that are usually not well-motivated from an experimental point of view.

The aim of the present paper is to present fresh results showing possibilities of modelling the onset of strain localisation and post-critical behaviour of granular materials within the framework of elastoplasticity, under the assumption of small strains and

rotations. In light of the above discussion, our study will follow three steps:

- A new constitutive model is proposed. This is based on broadly accepted concepts and is capable of describing the behaviour of granular materials under monotonic loading with a simple structure (smooth yield function and isotropic hardening, for instance), but maintaining features essential for the subsequent analysis. These features are incorporated through a novel use of elastoplastic coupling (Hueckel, 1976) and induced anisotropy, as described through a second-order fabric tensor (Valanis, 1990).
- Analysis of the onset of strain localisation is performed using standard concepts. This reveals the essential role played by induced elastic anisotropy, therefore extending previous results by Bigoni and Loret (1999) and Bigoni et al. (2000).
- Post-localisation analysis is investigated by developing a specific numerical procedure, based on certain simplifying assumptions (the width and inclination of the band are fixed, interaction of shear bands and boundary is neglected, the fields outside and inside the band are uniform). These allow a simple treatment of postcritical behaviour—somewhat inspired by Hutchinson and Tvergaard (1981), Tvergaard (1982) and Petryk and Thermann (2002)—without any addition to the constitutive law and without involving complex numerical treatments.

It is emphasised that, while the analyses by Hutchinson and Tvergaard (1981) and Petryk and Thermann (2002) refer to an infinite medium, our work attempts a direct comparison with experimental results. Thus, we refer to a finite specimen, where diffuse bifurcations become possible before strain localisation, but which is nevertheless assumed to remain homogeneous until the instant of localisation, a circumstance consistent—to within a certain approximation—with experimental results.

Though obtained using simplifying hypotheses,¹ the results of localisation analysis qualitatively and, more importantly, *quantitatively* agree with experimental results on dense sand, both in terms of onset of localisation and in terms of post-critical behaviour. In this respect, our constitutive model performs superiorly to all others known to us to describe granular materials. Important features emerge from the analysis of post-localisation, such as for instance, size effect of the sample and snap-back behaviour. Finally, a special, unexpected effect is shown to occur in both

¹ In principle, even under globally drained conditions, strain localisation may involve a locally undrained response. Therefore, in addition to the above setting, we assume also that the behaviour is locally and globally drained until and after strain localisation, a circumstance consistent with the high permeability of sands in relation to the relevant strain rates. From a theoretical point of view, analyses by Rice (1975), Loret and Harireche (1991) and Loret and Rizzi (1999) indicate that strain localisation is driven by the drained properties of the porous material. This appears to be substantiated by experimental results performed by Roger et al. (1998) by changing the pore fluid and the strain rate. Recently, however, Benallal and Comi (2003) have observed that strain localisation in undrained conditions could correspond to some kind of instability, related to the growth of perturbations in the underlying linearised problem. In our case, calculations not reported here indicate that localisation in undrained conditions may occur before localisation in drained conditions for loose sand only, where the behaviour is contractant (Gajo, 2003). A similar result was provided by Rudnicki (2001).

loose and dense sand as a function of the confining pressure, namely, *band saturation*. This occurrence was observed by Tvergaard (1982), who employed a version of the Gurson model for porous plastic metals, and consists in the ‘termination’ of a band (which elastically unloads) with the immediate formation of a new one in a different position within the material outside the initial band, which is now in a condition of plastic loading. Tvergaard did not suggest any physical interpretation for this and argued that it could represent a spurious effect related to the fact that nonassociative plastic response may be stiffer than elastic (Mróz, 1963, 1966).

The interpretation of the saturation mechanism requires the definition of a tool for analysing the post-saturation behaviour. This has been done in the present paper using a special numerical procedure, based on simplifying hypotheses. Results demonstrate that the following three principal mechanisms of localised deformation may occur in granular materials, showing surprisingly rich possibilities of continuation of material instability phenomena.

- A first mechanism, typical of dense sand, consists of the formation of a single shear band, initiating in the hardening regime and yielding a strong softening (with possible snap-back).
- A second mechanism is non-persistent band saturation. This mainly occurs in dense sand at low confining pressures and corresponds to the formation and subsequent saturation of a few shear bands, just preceding the formation of a (differently inclined) shear band occurring in the material transformed by the deformation developed in the initial shear bands. The global behaviour expressed in terms of nominal stress versus overall average axial strain exhibits a peak during hardening, corresponding to the initiation of the first shear band, followed by a few stress oscillations (denoting saturation), terminating in a strong softening (indicating the development of the final localisation). This deformation mechanism allows—in a sense—for a rotation of the shear band, which can eventually take an inclination very different from the initial one.
- The third and last deformation mechanism is peculiar to loose sand and corresponds to a persistent band saturation. This produces a continuing oscillation of nominal stress, so that the global behaviour is more or less reminiscent of ideal plasticity or, in other words, there are certain similarities with Lüders band formation in ductile metals (Hall, 1970) and phase transitions in shape memory alloy strips (Shaw and Kyriakides, 1997). More generally, the stress oscillation can be viewed as the effect of the repetition of a localised deformation mode, a situation occurring also in crushing of honeycombs (Papka and Kyriakides, 1999) and circular tubes subject to uniaxial compression (Bardi et al., 2003).

The variety of these deformation mechanisms clarifies some experimental results (Finno et al., 1997; Chambon and Desrues, 1986; Wong et al., 2001), which remained unexplained until now, but suggest also the possibility of existence of phenomena only partially revealed so far, so that the present work is intended also to stimulate the continuation of experimental research, particularly for the investigation of the second of the above mechanisms of deformation.

Notation

A standard notation is employed in this paper (for instance, see [Bigoni and Loret, 1999](#)), where bold letters denote vectors and second-order tensors. The scalar product between two vectors and second-order tensors, \mathbf{a} and \mathbf{b} is designated by $\mathbf{a} \cdot \mathbf{b}$ and the Euclidean norm of tensors and vectors by symbol $\|\cdot\|$. Moreover, tr is the trace operator, so that for generic second-order tensors \mathbf{A} and \mathbf{B} we have

$$\mathbf{A} \cdot \mathbf{B} = \text{tr} \mathbf{A} \mathbf{B}^T,$$

where a superscript T denotes transpose. The symbol \mathbf{I} indicates the second-order identity tensor and dev denotes the deviatoric component of a second-order tensor, so that

$$\text{dev} \mathbf{A} = \mathbf{A} - \frac{\text{tr} \mathbf{A}}{3} \mathbf{I}. \tag{1}$$

Given three arbitrary second-order tensors \mathbf{A}, \mathbf{B} and \mathbf{C} , we will make use of two tensorial products, the usual one

$$(\mathbf{A} \otimes \mathbf{B}) \mathbf{C} = (\mathbf{B} \cdot \mathbf{C}) \mathbf{A}, \tag{2}$$

and the following:

$$(\mathbf{A} \underline{\otimes} \mathbf{B}) \mathbf{C} = \frac{1}{2} (\mathbf{A} \mathbf{C} \mathbf{B}^T + \mathbf{A} \mathbf{C}^T \mathbf{B}^T), \tag{3}$$

so that the symmetrising operator \mathbb{S} may be written as

$$\mathbb{S} = \mathbf{I} \underline{\otimes} \mathbf{I}. \tag{4}$$

Note also that the following product between fourth-order tensors \mathbb{A} and \mathbb{B} will be employed

$$\mathbb{A} \mathbb{B}[\mathbf{A}] = \mathbb{A}[\mathbb{B}[\mathbf{A}]], \tag{5}$$

defined for every second-order tensor \mathbf{A} .

Two deviatoric invariants will often be employed throughout this paper, defined—for a generic tensor \mathbf{A} —as

$$J_{2(A)} = \frac{1}{2} \text{dev} \mathbf{A} \cdot \text{dev} \mathbf{A}, \quad J_{3(A)} = \frac{1}{3} \text{tr}(\text{dev} \mathbf{A})^3, \tag{6}$$

together with Lode’s angle invariant $\theta_{(A)}$

$$\theta_{(A)} = \frac{1}{3} \cos^{-1} \left(\frac{3\sqrt{3}}{2} \frac{J_{3(A)}}{J_{2(A)}^{3/2}} \right), \tag{7}$$

so that $\theta_{(A)} \in [0, \pi/3]$.

The constitutive model developed here is written in terms of effective stresses throughout and we omit for simplicity the prime often employed in soil mechanics to denote such stresses.

2. Constitutive modelling and elastoplastic coupling

Elastoplastic stress–strain relationships are proposed in this section to model the behaviour of granular materials under monotonic loading. Over a range of confining pressures in which grain crushing is excluded (below approximately 5–10 MPa, for common silica sand), mechanical behaviour of granular materials shows two basic features, namely,

- mean pressure and density dependency of elastic and plastic properties,
- smooth transition from very stiff response at very small strain to large plastic deformations near failure.

Several attempts have been made to include these features in a proper constitutive description. Recently, Gajo and Muir Wood (1999a,b) have proposed a kinematic hardening model, incorporating the parameter ψ introduced by Wroth and Bassett (1965) and Been and Jefferies (1985) to describe the dependency of current strength on current mean pressure and density. The constitutive model performs very well and accurately simulates the mechanical behaviour of granular materials in monotonic and cyclic loading tests, for a wide range of density and mean pressure levels. Employed to analyse strain localisation by Gajo et al. (2001), the model has provided an excellent simulation of the large dilatancy and associated decrease of strength occurring inside a shear band in dense sand. However, the elastic deformation in the model is not hyperelastic, so that inelastic deformation is produced both by plastic flow and by the specifically employed hypoelastic law. In addition, the model is rather complicated, so that it is not easy to understand which constitutive features are essential for the strain localisation analysis and which are needed to describe unrelated phenomena, such as for instance behaviour under cyclic loading.

In this paper we introduce a simplification on one hand and a generalization on the other of the Gajo and Muir Wood (1999a,b) model, which is reformulated by introducing a coupling between elastic and plastic deformation to describe state dependence of elastic behaviour without resorting to hypoelasticity. In particular, the main features of the model are:

- it is based on a single and smooth yield function,
- the flow rule is non-associative,
- the plastic response is strongly influenced by density and mean stress,
- there is a coupling between elastic and plastic deformations, the latter inducing progressive elastic anisotropy.

The concept of elastoplastic coupling, implicit in the work of Hill and Rice (1973); see also Hill (1978), was introduced by Hueckel (1975, 1976), Hueckel and Maier (1977), Maier and Hueckel (1979), Dougill (1976) and Dafalias (1977) with the aim of describing elastic degradation of rock-like materials, as induced by plastic deformation. The key idea is that it allows a description of progressive modifications of elastic properties, *within the framework of hyperelastic-plastic constitutive modelling*. Thus,

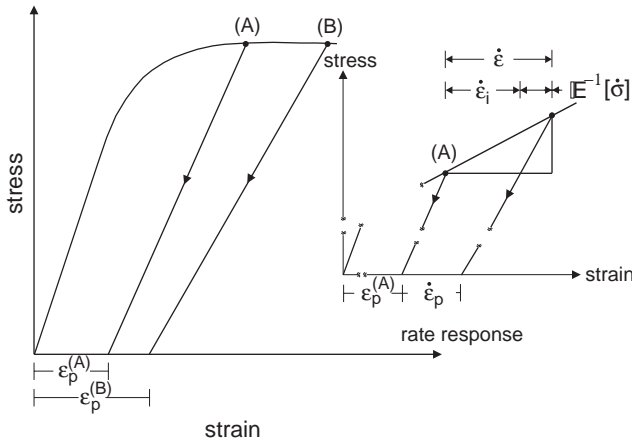


Fig. 1. Elastic stiffness degradation and elastoplastic coupling.

as shown in Fig. 1, elastic stiffness decreases when plastic deformation increases [so that the unloading stiffness starting from point (A) in Fig. 1 is higher than the unloading stiffness from point (B)]. The introduction of elastoplastic coupling allows one to avoid the usual assumption of hypoelasticity of the elastic branch of the constitutive law for modelling stiffness degradation. This is important since, because hypoelastic deformation may not be reversible in a finite cycle of loading, the distinction between elastic and plastic properties becomes simply impossible (see Maier and Hueckel, 1979, for details). We therefore exploit the framework of elastoplastic coupling to describe induced elastic anisotropy, as produced by particle reorientations and modifications of intergranular contacts, an effect that has been systematically tested in a conventional triaxial apparatus (Gajo et al., 2001; Gajo, 2004). Although not believed to be important in the description of the global stress–strain response of a soil sample, this becomes essential when the onset of shear banding is analysed (Bigoni and Loret, 1999; Bigoni et al., 2000).

2.1. The general structure of the constitutive equations

2.1.1. Yield function

The yield function

$$f = f(\boldsymbol{\sigma}, \boldsymbol{\alpha}), \tag{8}$$

is assumed to be a function of stress $\boldsymbol{\sigma}$ and internal variables $\boldsymbol{\alpha}$.

In order to define the specific functional form of the yield function (8), we refer to the critical state concept (Schofield and Wroth, 1968), the condition attained by granular materials after substantial deformations, in which shearing can continue without further changes in stress, density, volume, and pore pressure. In this steady state flow condition, the strength—described by the second stress invariant divided by a function of the Lode angle $\theta_{(\sigma)}$, namely, $\sqrt{J_{2(\sigma)}}/g(\theta_{(\sigma)})$ —represents a minimum for the granular medium and

(due to its frictional nature) may be described by the so-called ‘critical state friction angle’, ϕ_{cv} as

$$\frac{\sqrt{J_{2(\sigma)}}}{g(\theta_{(\sigma)})} = Mp, \quad M = \frac{2\sqrt{3} \sin \phi_{cv}}{3 - \sin \phi_{cv}}, \tag{9}$$

where $p = -\text{tr } \sigma/3$ is the mean pressure. Moreover, the specific volume at the critical state v_{cs} [defined as the ratio between the total volume and the volume of solid in a specimen, or 1/(solid volume fraction); $v = 1 + e$ where e is void ratio] depends only on the mean pressure in the following way

$$v_{cs} = v_A - A \ln p, \tag{10}$$

where v_A and A are two constitutive parameters. Note that relationships (9) and (10) define a surface in a p, v and $\sqrt{J_{2(\sigma)}/g(\theta_{(\sigma)})}$ coordinate system, providing a well-known graphical representation for the critical state condition. Usually, this surface is experimentally evaluated employing triaxial compression tests, so that determinations of the complete critical state surface are rare. Nevertheless Eqs. (9) and (10) have reached the status of unchallenged laws.

A significant feature of this model is that the density enters the formulation as a hardening parameter. In particular, we refer to the parameter ψ proposed by **Been and Jefferies (1985)** as

$$\psi = v - v_A + A \ln p, \tag{11}$$

representing a ‘volumetric’ measure of the distance of the current state from the critical state line, which corresponds to $\psi = 0$. Note that, within the framework of small strain theory and assuming that the solid grains are incompressible, the current specific volume in Eq. (11) may be written as

$$v = v_0(1 + \text{tr } \epsilon), \tag{12}$$

where v_0 is the initial specific volume, so that the state variable ψ depends through Eq. (11) on both the plastic and the elastic strain components. An additional hardening parameter, the accumulated octahedral plastic strain

$$\gamma_{\text{oct}}^p = \int_{\text{deformation path}} \sqrt{\frac{1}{3} \text{dev } \dot{\epsilon}^p \cdot \text{dev } \dot{\epsilon}^p}, \tag{13}$$

is introduced to complete the modelling of inelastic behaviour. This parameter is used to describe the smooth degradation of stiffness with progressive deformation, typical of granular material, through the following hyperbolic relationship, which is inspired by an equivalent function defined by **Gajo and Muir Wood (1999a,b)**

$$s(\gamma_{\text{oct}}^p) = 1 - \frac{B}{B/(1 - R) + \gamma_{\text{oct}}^p}, \tag{14}$$

where $R < 1$ and B are parameters, the former of which represents a measure of the initial size of the yield surface with respect to the size of the yield surface when the material reaches the peak strength.

We are now in a position to write down the (isotropic) yield function, dependent on the set of internal variables γ_{oct}^p and $\text{tr } \boldsymbol{\varepsilon}^p$ and stress $\boldsymbol{\sigma}$ as

$$f(\boldsymbol{\sigma}, \gamma_{\text{oct}}^p, \text{tr } \boldsymbol{\varepsilon}^p) = \sqrt{J_{2(\boldsymbol{\sigma})}} - (1 - k\psi) g(\theta_{(\boldsymbol{\sigma})}) M s(\gamma_{\text{oct}}^p) p, \tag{15}$$

where the dependence on $\text{tr } \boldsymbol{\varepsilon}^p$ is implicit in ψ , k is a positive constitutive parameter and function $g(\theta_{(\boldsymbol{\sigma})})$ is assumed in the form proposed by [Argyris et al. \(1974\)](#) (where $m > 0$ is a constitutive parameter)

$$g(\theta_{(\boldsymbol{\sigma})}) = \frac{2m}{1 + m + (1 - m) \cos 3\theta_{(\boldsymbol{\sigma})}}, \tag{16}$$

which is believed to provide a good match to experimental results.

Note that, since $\psi < 0$ for states below the critical state line, the peak strength of a material denser than at the critical state is greater than the strength at the critical state. The yield surface is an open non-circular cone for large deviatoric strains (i.e. $s(\gamma_{\text{oct}}^p) = 1$) and for a fixed value of $v_0(1 + \text{tr } \boldsymbol{\varepsilon}^p)$. It can be observed that, as a result of the chosen definition of the parameter ψ , the yield surface is mildly curved and lies above the critical state line at small mean pressure. At very high values of mean pressure or specific volume, the term $(1 - k\psi)$ becomes null or even negative, implying that the yield surface crosses the p -axis. Obviously, these values are meaningless, but if the model is properly calibrated they occur at large values of mean pressure or specific volume that have no practical meaning (since for these values either the mechanical behaviour would be dominated by grain crushing or the grain fabric would be much too loose to be stable). It should be finally noticed that the yield function has an implicit dependence on the stress, through parameter ψ , which is influenced by the elastic deformation.

2.1.2. Elastic potentials

As proposed by [Hill and Rice \(1973\)](#) and [Hueckel \(1976\)](#) the complementary free-energy density may in general depend not only on the stress $\boldsymbol{\sigma}$, but also on the entire history of plastic deformation reckoned from some reference state and represented in terms of an arbitrary set of internal variables. We limit here the presentation to the simple case in which the set reduces to the plastic strain $\boldsymbol{\varepsilon}^p$, so that

$$G = G(\boldsymbol{\sigma}, \boldsymbol{\varepsilon}^p), \quad \boldsymbol{\varepsilon} = \frac{\partial G}{\partial \boldsymbol{\sigma}}. \tag{17}$$

In particular, inspired by [Valanis \(1990\)](#) and [Bigoni and Loret \(1999\)](#), we assume

$$G(\boldsymbol{\sigma}, \boldsymbol{\varepsilon}^p) = \frac{1}{2} \boldsymbol{\sigma} \cdot \mathbb{E}^{-1}[\boldsymbol{\sigma}] + \boldsymbol{\sigma} \cdot \boldsymbol{\varepsilon}^p, \tag{18}$$

where the fourth-order tensor of current elastic moduli \mathbb{E} is defined, together with its inverse (on the space of all symmetric tensors), as

$$\begin{aligned} \mathbb{E} &= \lambda \mathbf{B} \otimes \mathbf{B} + 2\mu \mathbf{B} \underline{\otimes} \mathbf{B}, \\ \mathbb{E}^{-1} &= -\frac{\lambda}{2\mu(3\lambda + 2\mu)} \mathbf{B}^{-1} \otimes \mathbf{B}^{-1} + \frac{1}{2\mu} \mathbf{B}^{-1} \underline{\otimes} \mathbf{B}^{-1}, \end{aligned} \tag{19}$$

where λ and μ are constants (playing a role similar to Lamé coefficients of isotropic elasticity) satisfying the condition

$$\mu > 0, \quad \lambda + \frac{2}{3}\mu > 0, \tag{20}$$

and \mathbf{B} is a symmetric, second-order, positive definite tensor, describing fabric anisotropy, depending on the plastic strain $\boldsymbol{\varepsilon}^p$ and subject to the constraint

$$\text{tr } \mathbf{B}^2 = 3. \tag{21}$$

Obviously, when $\mathbf{B} = \mathbf{I}$ and for $\boldsymbol{\varepsilon}^p = \mathbf{0}$, the complementary energy of isotropic elasticity is recovered from Eq. (18).

The stress/strain relationships can be written in the form

$$\boldsymbol{\varepsilon} = \mathbb{E}^{-1}[\boldsymbol{\sigma}] + \boldsymbol{\varepsilon}^p, \quad \boldsymbol{\sigma} = \mathbb{E}[\boldsymbol{\varepsilon} - \boldsymbol{\varepsilon}^p]. \tag{22}$$

It should be noted that, since \mathbb{E} and \mathbb{E}^{-1} are dependent on the plastic strain $\boldsymbol{\varepsilon}^p$, the stiffness at unloading after plastic deformation has occurred is different from the elastic stiffness for a virgin loading, Fig. 1. This difference with respect to classical elastoplasticity represents the central concept of elastoplastic coupling (Hueckel, 1976). From Fig. 1 we may also note that the plastic strain $\boldsymbol{\varepsilon}^p$ takes the usual definition, namely, it is the residual strain when the stress vanishes.

Taking now the rate of Eqs. (22), we get

$$\dot{\boldsymbol{\varepsilon}} = \mathbb{E}^{-1}[\dot{\boldsymbol{\sigma}}] + \dot{\boldsymbol{\varepsilon}}^p - \mathbb{K}[\dot{\mathbf{B}}], \quad \dot{\boldsymbol{\sigma}} = \mathbb{E}[\dot{\boldsymbol{\varepsilon}} - \dot{\boldsymbol{\varepsilon}}^p] + \mathbb{H}[\dot{\mathbf{B}}], \tag{23}$$

where

$$\dot{\mathbf{B}} = \frac{\partial \mathbf{B}}{\partial \boldsymbol{\varepsilon}^p} [\dot{\boldsymbol{\varepsilon}}^p], \tag{24}$$

and the fourth-order tensor $\partial \mathbf{B} / \partial \boldsymbol{\varepsilon}^p$ is given in Appendix A. Tensors \mathbb{H} and \mathbb{K} appearing in Eq. (23) originate from elastoplastic coupling as

$$\begin{aligned} \mathbb{K} = & -\frac{\lambda}{2\mu(3\lambda + 2\mu)} [\mathbf{B}^{-1} \otimes \mathbf{B}^{-1} \boldsymbol{\sigma} \mathbf{B}^{-1} + (\mathbf{B}^{-1} \cdot \boldsymbol{\sigma}) \mathbf{B}^{-1} \underline{\otimes} \mathbf{B}^{-1}] \\ & + \frac{1}{2\mu} [\mathbf{B}^{-1} \boldsymbol{\sigma} \mathbf{B}^{-1} \underline{\otimes} \mathbf{B}^{-1} + \mathbf{B}^{-1} \underline{\otimes} \mathbf{B}^{-1} \boldsymbol{\sigma} \mathbf{B}^{-1}], \end{aligned} \tag{25}$$

$$\begin{aligned} \mathbb{H} = & \lambda [\mathbf{B} \otimes (\boldsymbol{\varepsilon} - \boldsymbol{\varepsilon}^p) + \mathbf{B} \cdot (\boldsymbol{\varepsilon} - \boldsymbol{\varepsilon}^p) \mathbf{I} \underline{\otimes} \mathbf{I}] \\ & + 2\mu [\mathbf{B} (\boldsymbol{\varepsilon} - \boldsymbol{\varepsilon}^p) \underline{\otimes} \mathbf{I} + \mathbf{I} \underline{\otimes} \mathbf{B} (\boldsymbol{\varepsilon} - \boldsymbol{\varepsilon}^p)], \end{aligned} \tag{26}$$

and satisfy the relation

$$\mathbb{H} = \mathbb{E} \mathbb{K}. \tag{27}$$

2.1.3. Plastic flow rule

From Eqs. (23) the rate of strain may be understood as the sum of a reversible $\mathbb{E}^{-1}[\dot{\boldsymbol{\sigma}}]$ and an irreversible strain rate $\dot{\boldsymbol{\varepsilon}}^i$, the latter being defined as the combination

of the plastic strain rate $\dot{\boldsymbol{\varepsilon}}^p$ and, say, a ‘coupling’ rate (see the detail of Fig. 1 for a geometrical interpretation of the rates)

$$\dot{\boldsymbol{\varepsilon}}^i = \mathbb{G}[\dot{\boldsymbol{\varepsilon}}^p], \quad (28)$$

where the coupling fourth-order tensor \mathbb{G} is defined as

$$\mathbb{G} = \mathbb{S} - \mathbb{K} \frac{\partial \mathbf{B}}{\partial \dot{\boldsymbol{\varepsilon}}^p}, \quad (29)$$

in which \mathbb{S} is the symmetrizing fourth-order tensor. The requirement of invertibility (on the space of all symmetric tensors) of the coupling tensor (29) has a self-evident importance, since it allows calculation of $\dot{\boldsymbol{\varepsilon}}^i$, when $\dot{\boldsymbol{\varepsilon}}^p$ is given. However, we require here that the coupling tensor \mathbb{G} be positive definite, the consequence of this is the fulfilment of the following ‘reasonable’ constraint inspired by Mróz (1963, 1966)

$$\dot{\boldsymbol{\varepsilon}}^p \cdot \dot{\boldsymbol{\varepsilon}}^i \geq 0. \quad (30)$$

Positive definiteness of \mathbb{G} has to be regarded as a feature limiting the extent of elasto-plastic coupling. A way in which the values of constitutive parameters can be bounded in order to ensure positive definiteness of \mathbb{G} is given in Appendix B. The bound suggests that the tensor is always positive definite a priori for stiff materials like concrete, rocks or dense sand, but for soft materials like loose sand, the bound is not very effective, so that the satisfaction of positive definiteness has to be checked along a given deformation path.

Obviously, plastic and irreversible deformations are different and related by the following equation, obtained from integration of Eq. (28)

$$\boldsymbol{\varepsilon}^i = \int_{\text{deformation path}} \mathbb{G}[\dot{\boldsymbol{\varepsilon}}^p] = \boldsymbol{\varepsilon} - \int_{\text{deformation path}} \mathbb{E}^{-1}[\dot{\boldsymbol{\sigma}}]. \quad (31)$$

The choice of the plastic deformation as an internal variable in the yield function (8) instead of the irreversible deformation may seem arbitrary, but may be justified by observing that in a finite loading–unloading cycle starting from a null stress state, only the former has a clear physical meaning. Considering an infinitesimal loading–unloading cycle, the irreversible strain variation represents the net residual strain at the end of the cycle. Following Hill and Rice (1973), since the plastic flow rule is defined through a flow mode tensor usually corresponding to the net residual strain in an infinitesimal loading–unloading cycle, it may appear natural to assume [as in Collins and Houslyby, 1997; Bigoni, 2000; and differently from Hueckel, 1976; Capurso, 1979; Hueckel and Maier, 1977; Maier and Hueckel, 1979; Bigoni and Hueckel, 1991; Brannon and Drugan, 1993]

$$\dot{\boldsymbol{\varepsilon}}^i = \dot{\gamma} \mathbf{P}, \quad (32)$$

where $\dot{\gamma} \geq 0$ is the plastic multiplier and \mathbf{P} the (symmetric) flow mode tensor. The choice of condition (32) is a constitutive assumption, so that it is to a certain extent arbitrary. However, the choice becomes crucial, since it implies symmetry of the tangent constitutive operator when normality holds true, or in other words, when \mathbf{P} coincides with the yield function gradient.

For simplicity we use deviatoric associativity and, following Gajo and Muir Wood (1999b), we assume

$$\frac{\text{tr } \mathbf{P}}{\|\text{dev } \mathbf{P}\|} = -\sqrt{3}A \left[(1 + k_d \psi) M - \frac{\sqrt{J_{2(\varepsilon^p)}}}{g(\theta_{(\varepsilon^p)})} p \right], \tag{33}$$

where A and k_d are constitutive parameters. Eq. (33) completely defines the tensor \mathbf{P} .

2.1.4. Hardening rule

On the basis of the assumed yield function, the following hardening rule is selected

$$H = -v_0 \frac{\partial f}{\partial \psi} \mathbf{I} \cdot \mathbb{G}^{-1}[\mathbf{P}] - \frac{1}{\sqrt{3}} \frac{\partial f}{\partial \gamma_{\text{oct}}^p} \|\text{dev } \mathbb{G}^{-1}[\mathbf{P}]\|. \tag{34}$$

where H is the plastic modulus, depending on the current state through $\boldsymbol{\sigma}$ and ε^p .

2.1.5. The rate constitutive equations

Prager’s consistency condition $\dot{f} = 0$ yields the plastic multiplier

$$\dot{\gamma} = \frac{\mathbf{Q} \cdot \mathbb{E}[\dot{\boldsymbol{\varepsilon}}]}{\mathbf{Q} \cdot \mathbb{E}[\mathbf{P}] + H}, \tag{35}$$

where \mathbf{Q} is the gradient of the yield function

$$\mathbf{Q} = \frac{\partial f}{\partial \boldsymbol{\sigma}}. \tag{36}$$

A substitution of Eq. (35) into Eqs. (32) and (23)₂ gives the usual form of the elasto-plastic incremental constitutive laws

$$\dot{\boldsymbol{\sigma}} = \mathbb{E}[\dot{\boldsymbol{\varepsilon}}] - \frac{\langle \mathbf{Q} \cdot \mathbb{E}[\dot{\boldsymbol{\varepsilon}}] \rangle}{H + \mathbf{Q} \cdot \mathbb{E}[\mathbf{P}]} \mathbb{E}[\mathbf{P}], \tag{37}$$

in which the Macaulay bracket operator is defined for every $\alpha \in \Re$ as $\langle \alpha \rangle = (\alpha + |\alpha|)/2$. The tangent operator corresponding to the loading branch of Eq. (37) has the usual structure

$$\mathbb{C} = \mathbb{E} - \frac{1}{H + \mathbf{Q} \cdot \mathbb{E}[\mathbf{P}]} \mathbb{E}[\mathbf{P}] \otimes \mathbb{E}[\mathbf{Q}], \tag{38}$$

so that, as in Bigoni (2000), symmetry is recovered for an associative flow rule, when $\mathbf{P} = \mathbf{Q}$. Note that the elastoplastic coupling enters Eq. (38) through the dependence of the elastic tensor \mathbb{E} on the plastic strain.

2.2. The fabric tensor

The dependency of the fabric tensor \mathbf{B} on the plastic strain ε^p is assumed in such a way that the two tensors are coaxial. In particular, the following expression has been employed

$$\mathbf{B} = -\beta \text{dev } \varepsilon^p + \sqrt{\frac{3 - 2J_{2(\varepsilon^p)}\beta^2}{3}} \mathbf{I}, \tag{39}$$

where the function $\beta = \beta(J_{2(\epsilon^p)}, \theta_{(\epsilon^p)})$ depends on the plastic strain (namely on the second invariant $J_{2(\epsilon^p)}$ and Lode angle invariant $\theta_{(\epsilon^p)}$, see Eq. (7), of the plastic strain) according to

$$\beta(J_{2(\epsilon^p)}, \theta_{(\epsilon^p)}) = \frac{A_\epsilon g(\theta_{(\epsilon^p)})}{B_\epsilon g(\theta_{(\epsilon^p)}) + \sqrt{2J_{2(\epsilon^p)}}}, \tag{40}$$

with

$$g(\theta_{(\epsilon^p)}) = \frac{2m_\epsilon}{1 + m_\epsilon + (1 - m_\epsilon) \cos 3\theta_{(\epsilon^p)}}, \tag{41}$$

and A_ϵ, B_ϵ and m_ϵ are nonnegative constitutive parameters. In this way a hyperbolic relationship is introduced between the deviatoric component of \mathbf{B} and the deviatoric component of ϵ^p . At zero deviatoric plastic strain, the anisotropy is zero and $\mathbf{B} = \mathbf{I}$, whereas at very large deviatoric plastic strains, the fabric tensor \mathbf{B} reaches a saturation condition. Note that elastic isotropy is recovered when $A_\epsilon = 0$ and the elasto-plastic coupling disappears.

The inverse tensor \mathbf{B}^{-1} , can be easily obtained by using the Cayley–Hamilton theorem:

$$\mathbf{B}^{-1} = \frac{1}{\det \mathbf{B}} \left[\beta^2 (\text{dev } \epsilon^p)^2 + \beta \sqrt{\frac{3 - 2J_{2(\epsilon^p)}\beta^2}{3}} \text{dev } \epsilon^p + \frac{3 - 5J_{2(\epsilon^p)}\beta^2}{3} \mathbf{I} \right]. \tag{42}$$

The following restriction is imposed to ensure positive definiteness of the fabric tensor \mathbf{B} (obtained in Appendix C)

$$0 \leq g(\theta_{(\epsilon^p)}) A_\epsilon \leq \frac{1}{\sqrt{\frac{1}{3} + \frac{1}{2(1+\rho+\rho^2)}}} \leq \sqrt{2}, \tag{43}$$

where $-2 \leq \rho \leq -1/2$ is the ratio between the minimum and maximum eigenvalues of the deviatoric plastic strain.

In conclusion, for describing the evolution of elastic anisotropy within the framework of elasto-plastic coupling, three parameters (B_ϵ, A_ϵ and m_ϵ) are necessary. The three parameters are physically well anchored and their calibration from experimental results will be described in Appendix D. In particular, since our aim is a direct comparison with experiments, it can be understood that the calibration of the constitutive parameters of the above-described constitutive model plays an important role. While the calibration of the main parameters has been obtained from data already known, the evaluation of the parameters needed to describe the evolution of elastic anisotropy has required the development of an experimental technique. Details on the calibration are deferred in Appendix D.

3. Strain localisation analysis

3.1. Initiation of strain localisation

The initiation of strain localisation is understood here in the usual sense (Rice, 1977) as the singularity of the acoustic tensor corresponding to the loading branch of

the elastoplastic operator given by Eq. (38), namely

$$\mathbf{A}_{ep}(\mathbf{n})\mathbf{g} = \mathbb{C}[\mathbf{n} \otimes \mathbf{g}]\mathbf{n}, \tag{44}$$

defined for all unit vectors \mathbf{n} and all non-zero vectors \mathbf{g} . It is important to remark that we exclude here the possibility that the elastic acoustic tensor can be singular (corresponding to a purely elastic strain localisation), so that in a loading program controlled by a monotonically increasing loading parameter and starting from a situation in which the acoustic tensor is positive definite, the first possibility of strain localisation always occurs at the singularity of acoustic tensor (44) and corresponds to plastic loading inside the band and neutral loading outside (Rice and Rudnicki, 1980; Bigoni and Zaccaria, 1993). Imposing singularity of the acoustic tensor (44) yields a well-known constrained maximisation problem, defining the critical hardening modulus h_{cr} for strain localisation

$$h_{cr} = \max_{\mathbf{n}, |\mathbf{n}|=1} \{ \mathbb{E}[\mathbf{Q}]\mathbf{n} \cdot \mathbf{A}_e^{-1}(\mathbf{n})\mathbb{E}[\mathbf{P}]\mathbf{n} \} - \mathbf{Q} \cdot \mathbb{E}[\mathbf{P}], \tag{45}$$

where \mathbf{A}_e is the elastic acoustic tensor. The maximisation problem (45) was explicitly solved by Rudnicki and Rice (1975) for isotropic elasticity and coaxial yield function and plastic potential gradients. Bigoni and Loret (1999) and Bigoni et al. (2000) have analysed the problem of elastic anisotropy relevant to the present paper. Their solutions can be used when tensors \mathbf{P} , \mathbf{Q} and \mathbf{B} are coaxial, a condition which may not be verified in our model for general loading, but it is verified if we refer to the state of stress realized in a biaxial or triaxial test apparatus. Therefore, the condition for the onset of strain localisation will be obtained analytically in the examples that follow using formulae taken from Bigoni et al. (2000) and not repeated here for conciseness. It is important however to realise that the specific elastic anisotropy evolution introduced in our model is a key feature in determining the onset of strain localisation, particularly for simulation of triaxial tests (Gajo et al., 2004).

3.2. Post-localisation analysis

Following Hutchinson and Tvergaard (1981), the analysis of the post-localisation regime can be performed assuming the existence of two distinct homogeneous solutions, one outside the band (deformation labelled $\boldsymbol{\varepsilon}_o$) and the other inside the band (deformation labelled $\boldsymbol{\varepsilon}_i$), the increment of which must satisfy at every instants Maxwell kinematic compatibility conditions, so that

$$\dot{\boldsymbol{\varepsilon}}_i = \dot{\boldsymbol{\varepsilon}}_o + \frac{1}{2}[\mathbf{g} \otimes \mathbf{n} + \mathbf{n} \otimes \mathbf{g}], \tag{46}$$

where vector \mathbf{n} is fixed and initially obtained imposing the singularity of the acoustic tensor, Eq. (45), whereas vector \mathbf{g} is obtained imposing global compatibility for a specimen in a way that will be explained later. In addition to condition (46), stress compatibility requires continuity of tractions at every instant (and thus also continuity of traction rates) across the interface

$$\boldsymbol{\sigma}_o\mathbf{n} = \boldsymbol{\sigma}_i\mathbf{n}, \quad \rightsquigarrow \quad \dot{\boldsymbol{\sigma}}_o\mathbf{n} = \dot{\boldsymbol{\sigma}}_i\mathbf{n}. \tag{47}$$

We refer for simplicity to a small strain regime and we assume that the shear band is planar with constant inclination and thickness. While the band inclination is found

from the solution of the condition of singularity of the acoustic tensor, *the thickness of the band is simply imposed*, assuming values deduced from experimental observation (Roscoe, 1970; Muir Wood, 2002). In the post localisation regime, because the material inside and outside the band can undergo either elastic unloading or plastic loading, four different cases may exist. Referring to the acoustic tensors of the material inside (denoted by index i) and outside (denoted by index o) the band, equipped with indices e and ep to specify the elastic and the tangent elastoplastic responses, Eqs. (46) and (47) yield the four conditions that follow, referred to a generic instant of post-critical behaviour, when the band is already formed.

- Plastic loading outside and inside the band

$$A_i^{ep}(\mathbf{n})\mathbf{g} = C_o[\dot{\epsilon}_o]\mathbf{n} - C_i[\dot{\epsilon}_o]\mathbf{n}, \tag{48}$$

- Plastic loading outside and elastic unloading inside the band

$$A_i^e(\mathbf{n})\mathbf{g} = C_o[\dot{\epsilon}_o]\mathbf{n} - E_i[\dot{\epsilon}_o]\mathbf{n}, \tag{49}$$

- Elastic unloading outside and plastic loading inside the band

$$A_i^{ep}(\mathbf{n})\mathbf{g} = E_o[\dot{\epsilon}_o]\mathbf{n} - C_i[\dot{\epsilon}_o]\mathbf{n}, \tag{50}$$

- Elastic unloading outside and inside the band

$$A_i^e(\mathbf{n})\mathbf{g} = E_o[\dot{\epsilon}_o]\mathbf{n} - E_i[\dot{\epsilon}_o]\mathbf{n}. \tag{51}$$

Although the second and the fourth of the above possibilities may seem unrealistic, the second will be found to occur and to be crucial in understanding the band saturation process and the fourth may also occur in the post-saturation analysis as a consequence of the evolution of elastic properties, resulting from elastoplastic coupling.

It is now possible to proceed following Hutchinson and Tvergaard (1981), Tvergaard (1982) and Petryk and Thermann (2002) with reference to an infinite medium, in which the band thickness becomes inessential. However, our intention is to achieve a direct comparison with experimental results, obtained from biaxial, plane strain experiments. Therefore, we introduce certain strong simplifying hypotheses, which we believe do not alter the qualitative results. In particular, we refer to a finite, rectangular specimen of initial height L_0 , deformed in plane strain with a prescribed velocity \dot{u}_1 in the (vertical) direction singled out by unit vector \mathbf{e}_1 and containing a band of initial thickness s_0 . Therefore, the plane strain condition (in the direction 3) and the vanishing of the loading rate along the boundary parallel to \mathbf{e}_1 (having unit normal in the direction 2) are

$$\dot{\epsilon}_{33} = 0, \quad \dot{\sigma}_{22} = 0. \tag{52}$$

The behaviour is assumed homogeneous until the instant of localisation, so that the effects of all the diffuse bifurcations that in a finite specimen may occur before localisation are neglected. The available experimental results suggest in fact that such bifurcations are actually likely to occur, but do not much alter the overall behaviour, which remains dominated by the localisation phenomena. In these conditions, when a band of localised deformations is considered, a ‘global’ kinematic condition must be

imposed for the deformed block, expressing the fact that the height variation of the block is the sum of the contributions inside and outside the band. This condition allows the determination of the modulus of \mathbf{g} and can be written as

$$L_0 \dot{\varepsilon}_{11}^0 + s_0 \mathbf{g} \cdot \mathbf{e}_1 = \dot{u}_1, \quad (53)$$

where $\dot{\varepsilon}_{11}^0$ is the component of $\dot{\varepsilon}_0$ along the axis of load.

A numerical integration of the constitutive rate equations before and after localisation can now be performed (see Gajo, 2003 for details). Briefly, for homogeneous response, the stress at the end of each integration step (in general) violates the yield condition, which has therefore to be enforced. This is obtained introducing a generalization of the cutting plane algorithm (Simo and Hughes, 1987), needed since the simulation of biaxial testing requires a mixed prescription of strain and stress. The same problem occurs after strain localisation outside the band, whereas inside the band different prescriptions arise from requirements that the tractions be continuous across the band and the deformation rate be in form (46).

During the process of post-localisation (as a result of the small strain hypothesis) the band inclination \mathbf{n} remains fixed, while \mathbf{g} is allowed to change both in direction and modulus. At a generic step of the numerical integration in the post-localisation regime, all Eqs. (48)–(51) hold true when the stress states inside and outside the band lie on the yield surface. In this case, all the mechanisms of deformation represented by Eqs. (48)–(51) are separately considered, according to the following procedure, referred for simplicity to the plastic/plastic mechanism, but which can be easily understood in all the other particular cases.

- The vertical incremental displacement Δu_1 is assigned and a tentative $\Delta \varepsilon_{11}^0$ is assumed;
- $\Delta \varepsilon_{22}^0$ is evaluated from the condition $\Delta \sigma_{22} = 0$, using the tangent constitutive operator \mathbb{C}_0 . Consequently, $\Delta \varepsilon_0$ is known;
- imposing Eq. (48), \mathbf{g} is calculated, so that $\Delta \varepsilon_i$ is known;
- the conditions of plastic loading are checked inside and outside the band. If one of these is violated, the procedure is terminated and another deformation mechanism is analysed. Otherwise, the current mechanism is considered possible and the exact value of $\Delta \varepsilon_{11}^0$ is obtained from equation (53). Finally, all quantities are re-scaled to the correct values (this is an immediate operation since all equations are here linear).

It is possible that more than one mechanism of localised deformation is detected from the above screening. In such cases a stability requirement could be employed to select one. However, in the present context of nonassociative, coupled elastoplasticity, not much is known about proper stability criteria (Bigoni, 2000). We therefore employ a heuristic criterion, by which the deformation mechanism corresponding to the steepest descent in the global force versus displacement curve for the sample is selected. The selection is performed using the linearised equations. At the end of this screening, a tentative solution of the linearised problem is found. On the basis of this, a refined incremental solution is calculated enforcing the yield condition within a given strict

tolerance, employing again the extension of the cutting plane algorithm just mentioned. In this case however, the extension is needed to satisfy the condition that the stress state inside the band must satisfy the requirement of continuity of tractions across the band. Therefore, the boundary conditions at the points where the band emerges on the edges of the sample are violated. Moreover, since the iterations with the cutting plane algorithm slightly modify the values of the strain inside the band, at the end of the integration step Maxwell kinematic compatibility conditions (Eq. (46)) will not be perfectly satisfied inside the band. If the error in terms of strain is large, then the strain increment necessary to satisfy Maxwell kinematic compatibility conditions is applied inside the band, by using an implicit backward-Euler integration algorithm. Convergence was ensured through the use of the line search procedure, adjusting any Newton step ending excessively far from the solution (Matthies and Strang, 1979; Johan et al., 1991).²

3.2.1. Numerical results and comparison with experiments

A typical simulation of a drained biaxial test (in which the vertical compressive strain is increased and a constant horizontal stress is maintained) performed on a 350 mm high sample of dense³ Hostun sand ($e = 0.673$) at a confining pressure of 400 kPa is shown in Fig. 2. Note that with ‘confining pressure’ p_0 we mean here and in the following the *initial* in-plane confining pressure, defined as the sum of the vertical and horizontal initial stresses divided by 2. Moreover, stresses and strains are represented positive when corresponding to compression in Fig. 2 and in all plots that follow. A band inclined at 34.5° (here and throughout the paper angles referring to shear band inclinations are measured from the vertical) has been found to occur in the hardening regime. The ‘global’ response of the specimen is represented in the figure, in the sense that the nominal stress (applied axial load resultant divided by the initial cross sectional area of the sample) and the conventional volumetric strain (total volume variation divided by the initial volume of the sample) are reported in Figs. 2(a) and (b), as a function of the conventional strain (axial sample shortening divided by the original height of the sample). In other words, the plots represent the interpretation that would be given for the test ignoring the fact that the deformation has become localised. The homogeneous response (represented with a dashed line after the initiation of localisation) is also included in the figure. The thickness of the shear band has been assumed equal to 6 mm, corresponding to 15 grain diameters, a value suggested by experiments (Roscoe, 1970; Muir Wood, 2002).

First of all, it can be observed from the figure that the localisation of deformation changes the results qualitatively. Because of the non-normality of the flow rule, strain

² A few iterations have been found to be sufficient for reaching a strict tolerance on residuals. However, this will be not the case when band saturation is involved. In fact, the elasto-plastic acoustic tensor inside the band, Eq. (50), may become singular when band saturation occurs. In this case, the final residual strain increment is evaluated by using the cutting plane algorithm (imposing strain increments only and consequently accepting a small error on the continuity of traction across the interface between inside and outside the band), instead of the above-described implicit backward-Euler integration algorithm. A maximum value of 1 Pa in the norm of the residual traction at band interface was tolerated in our computations.

³ Dense and loose sands are discriminated here on the basis of the dilatant or contractant behaviour.

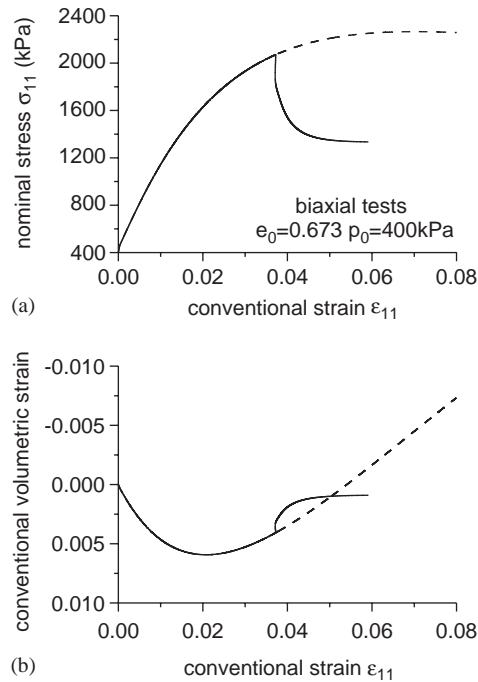


Fig. 2. Simulation of the ‘global’ response of a 350 mm high sample of dense sand at high confining pressure. (a) nominal axial stress versus conventional strain, (b) conventional volumetric versus axial strain.

localisation initiates in the hardening regime and soon leads to a large softening, so that the *conventional* sample strength is significantly lowered. At the instant of localisation, the condition of neutral loading outside the band and plastic loading inside occurs. This phase is immediately followed by elastic unloading outside the band, giving rise to the global abrupt softening. It may be important to realize that the softening partially originates from the peculiar kinematics involved with strain localisation (so that it may occur also when the material does not exhibit softening, as in the case of loose sand) and partially from softening occurring inside the band due to dilatant volumetric strains.

Studying Fig. 2(b), we may note that the sample experiences an initial contraction, soon followed by dilation, but this is strongly reduced in the post-localisation regime. Inside the band, the material undergoes a large dilation, which induces the global softening, until the critical state condition is obtained within the band. In order to illustrate the primary role played by the variable ψ , describing the dependence of sand from density (pycnotropy), we report in Fig. 3 the variation of ψ inside and outside the shear band, relative to the example presented in Fig. 2. There is a large increase of ψ inside the shear band and a corresponding decrease in strength, while ψ remains almost constant outside the band.

Typical experimental results obtained by Desrues and Hammad (1989) on dense Hostun sand at different pressures ($p_0 = 100, 200, 400,$ and 800 kPa) are reported in

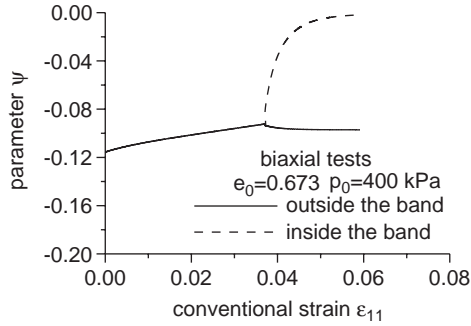


Fig. 3. Variation of the parameter ψ describing density dependence of strength inside and outside the band, with reference to Fig. 2.

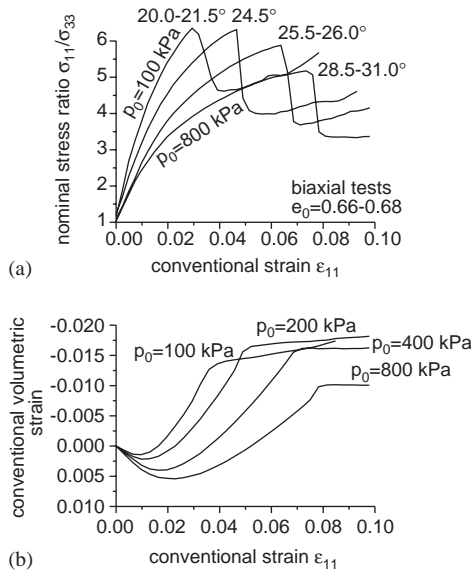


Fig. 4. Experimental results on samples of dense Hostun sand at different confining pressure (taken from Desrues and Hammad, 1989). (a) nominal axial stress versus conventional strain, (b) conventional volumetric versus axial strain.

Fig. 4. The figure can be directly compared with the simulations reported in Fig. 5 for the same values of pressure. It is evident that the qualitative and quantitative behaviour is correctly described by the model. We may note, in particular, that increasing the pressure decreases the band inclination both in the experiments (where it ranges between 20° at $p_0 = 100$ kPa and 31° at $p_0 = 800$ kPa) and in the simulations (from 33.8° at $p_0 = 100$ kPa to 35.0° at $p_0 = 800$ kPa). Although the values of band inclination are overestimated by the model, the values of peak loads and their decrease with increasing pressure are well captured.

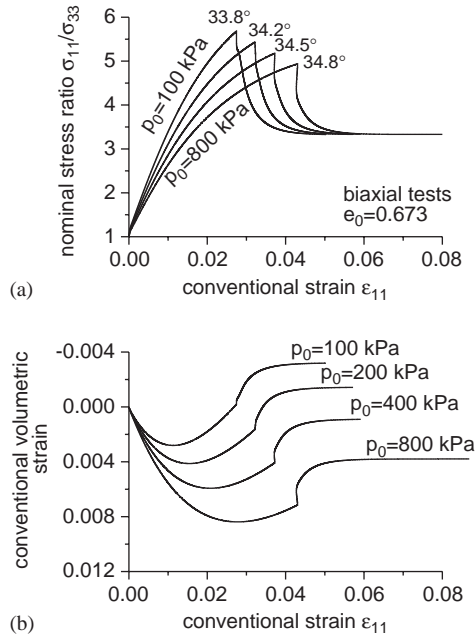


Fig. 5. Simulations of experimental results for dense Hostun sand reported in Fig. 4. (a) nominal axial stress versus conventional strain, (b) conventional volumetric versus axial strain for different values of confining pressure.

The band inclination and the post-critical behaviour are *predictions* of the model. In all the simulations the bands are found to be consistently less steep (nearer to the horizontal) than in the experimental observations: this is the most apparent discrepancy between prediction and experiments. In the geotechnical literature, there are three relations which are thought to provide a fit of experimental results on shear band inclinations. The inclinations are given by $\pi/4 - \alpha/2$, where α is the friction angle in the so-called ‘Coulomb’ model, is the dilatancy angle in the Roscoe model (Roscoe, 1970) and is approximately the mean of friction and dilatancy angles in the Arthur et al. (1977) model [the latter has been validated by Vardoulakis, 1980, 1988].

Following these expressions, the expected inclinations range between 22° and 25° for the Coulomb model, between 39° and 42° for the Roscoe model and between 31° and 33° for the Arthur model, for confining pressures between 100 and 800 kPa. We conclude that our model predictions are close to the Arthur inclinations, whereas the observations lie closer to the Coulomb result at low confining pressure.

A constant value of nominal stress is reached during the post-critical behaviour in the model prediction, while the load reaches a minimum and then increases again in the experiments. Such an effect may be linked with the detail of the membrane/soil interaction and may not necessarily be a consequence of material behaviour. The inclusion in the simulations of the membrane interaction induces also an out-of-plane compliance delaying the onset of localisation. A detailed analysis of these effects is reported elsewhere (Gajo et al., 2004).

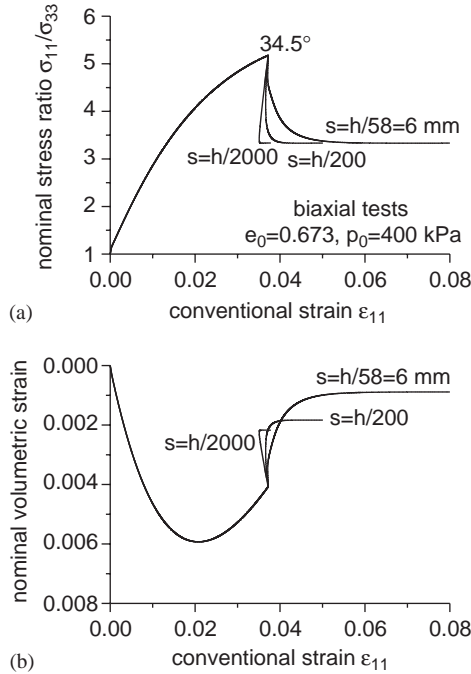


Fig. 6. Simulation of the ‘global’ response of a 350 mm high sample of dense sand for different band thickness. (a) nominal axial stress versus conventional strain, (b) conventional volumetric versus axial strain. A strong size effect and related snap-back behaviour is clearly visible.

The ratio between sample height and band thickness ($h/s = 350/6 \approx 58$) employed in the simulations reported in Figs. 2 and 5 corresponds to that observed in the experiments. However, the simulations are strongly affected by the value of this ratio, so that a *size-effect* is clearly exhibited (a feature also discussed by Needleman, 1988, in a unidimensional context). Results are reported in Fig. 6 for different values of $h/s = 58, 200, 2000$. Obviously, while the minimum thickness of the shear band may be dictated by microstructural considerations, the scale of the problem may change the ratio h/s up to, say, infinity, at least when compared with the typical value of band thickness. It may be observed from the figure that the higher the ratio h/s , the steeper is the global softening experienced by the sample. In particular, snap-back is observed for both the values $h/s = 200$ and 2000 , for which the stress dynamically drops from the peak value to the value corresponding to residual sample strength (note also the jump in the volumetric behaviour reported in Fig. 6(b)). The softening branch tends to coincide with the elastic unloading stiffness in the limit $h/s \rightarrow \infty$.

3.3. Band saturation

In addition to the shear band mechanism described in the previous section, an unexpected mechanical behaviour is also observed to occur in both dense and loose

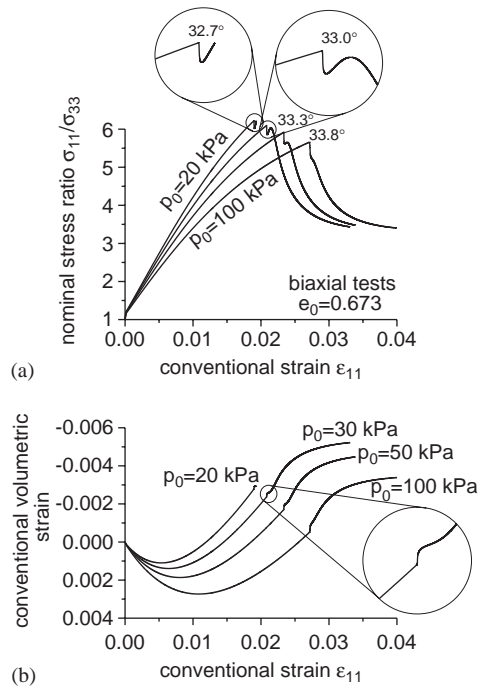


Fig. 7. Simulation of the 'global' response of a 350 mm high sample of dense sand at low confining pressures. (a) nominal axial stress versus conventional strain, (b) conventional volumetric versus axial strain.

sand, depending on the value of the confining pressure. For dense sand, in particular, an analysis of the response at a confining pressure lower than the minimum value analysed in the previous section, yields the behaviour reported in Fig. 7, for $p_0 = 20, 30, 50, 100$ kPa. In particular, initially the usual mechanism of elastic unloading outside the band and plastic loading inside prevails after localisation, yielding a steep softening behaviour. However, the load reaches a minimum where softening terminates and the response again exhibits positive hardening. This hardening phase is very short and, depending on the confining pressure, it may just evolve into a maximum (at which the acoustic tensor becomes singular in a direction parallel to the band) preceding again a new softening phase or it may continue until the load becomes equal to that at which localisation initiated (Fig. 7). In this case, the material outside the band reaches the yield condition and is immediately at the condition of strain localisation reached when the first band occurred. At this point, a localisation occurs outside the band (in the zone where the material had elastically unloaded and then reloaded) and all the rest of the material elastically unloads, including the material which was plastically deforming inside the initial band. This behaviour is evident in the conventional stress–strain curves reported in Fig. 7, where the band inclinations $32.7^\circ, 33.0^\circ, 33.3^\circ, 33.8^\circ$ correspond, respectively, to the confining pressures 20, 30, 50 and 100 kPa. Note that the curve for the band inclination 32.7° is interrupted when the condition of elastic

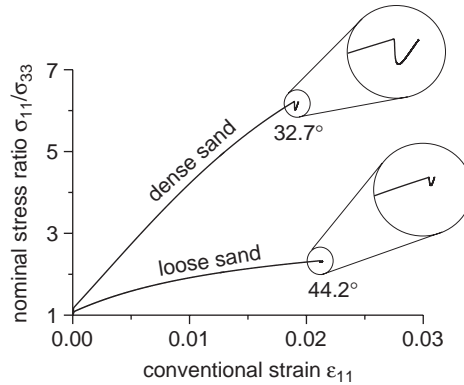


Fig. 8. Simulation of the ‘global’ response of 350 mm high samples of dense sand at low (20 kPa) and loose sand at high (100 kPa) confining pressure. Nominal axial stress versus conventional strain.

unloading in the initial band occurs, whereas this condition is not attained in all the other curves. An analogous behaviour has also been observed (but is not shown here) for loose sand (defined here as a sand undergoing volumetric contraction) at any range of confining pressure (provided the volumetric behaviour remains contractive).

Tvergaard (1982) found similar behaviour to occur in a porous plastic material and denoted it *band saturation*. He suggested that it could be related to the fact that the elasto-plastic stiffness may be higher than the elastic stiffness for a material with a nonassociative flow rule (Mróz, 1963, 1966). Following Tvergaard, we checked the elasto-plastic stiffness during our simulations, but this was only seldom found to be higher than the elastic stiffness. Therefore, we believe that this should not be the leading mechanism of band saturation, at least for the strain rate directions involved in our analysis.

Band saturation is the result of two very different effects in loose and dense sand. Fig. 8 shows the simulation of a dense sand (corresponding to band inclination 32.7° and $e_0 = 0.673$) and a loose sand (corresponding to band inclination 44.3° and $e_0 = 0.914$) tested at confining pressures of 20 and 100 kPa, respectively. The deformation inside the band for the two kinds of sand considered in Fig. 8 is reported in Fig. 9 as a function of the conventional axial strain. Normal versus shear deformation components inside the band are reported in the details of the figure. For the loose sand, the material inside the band undergoes volumetric contraction and consequently hardens (Fig. 9), so that the material inside the band acquires a strength higher than that outside and this yields a decrease of the deformation inside the band, giving rise to saturation. This mechanism finds experimental confirmation, as will be shown in the next section.

Band saturation in dense sand is, however, a less easily understood phenomenon than in loose sand, since the material inside the band undergoes volumetric expansion (Fig. 9) and consequently softens, so that an increase in the resulting load is not expected at a first glance. The rate of softening, however, is the result of the kinematic and static constraints imposed by the band and mainly depends on band inclination,

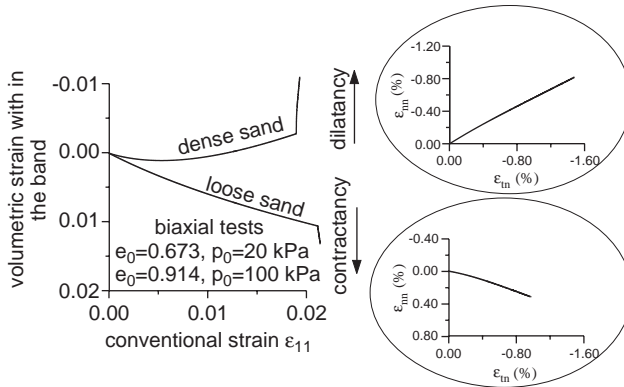


Fig. 9. Simulation of the ‘global’ response of 350 mm high samples of dense sand at low (20 kPa) and loose sand at high (100 kPa) confining pressure. Volumetric deformation inside the band versus conventional strain. Normal versus shear deformation components inside the band for dense and loose sand are displayed in the details.

plastic volumetric compressibility (i.e. on model parameter A), and the elastic stiffness of the material outside the band. The link between volumetric strain and shear strain (the strain path) within the band is shown in the inset detail of Fig. 9, where it becomes evident that the rate of volumetric expansion is fairly constant in the early phases of straining, during which band saturation occurs. Note from the detail of Fig. 9 that band saturation occurs at small strains inside the band (1.5% or smaller), thus supporting the small strain assumption and the consequent neglect of the stiffness increase related to possible finite rotations.

In order to gain a better understanding of the behaviour of dense sand inside the band, the homogeneous response has been analysed for a material having approximately the same initial conditions (of density, deformation and stress states) and subject to the same deformation path as a material element inside the band. Results are reported in Fig. 10 for the homogeneous response of a material element subject to a simple shear test at the same, constant, ratio $\epsilon_{11}/\epsilon_{12}$ between the volumetric and shear strains that is observed to occur within the band (see the detail in Fig. 9). Fig. 10 shows the response of a dense sand with $e_0 = 0.673$, for three different values of $\epsilon_{11}/\epsilon_{12} = \{0.38, 0.48, 0.57\}$, computed for initial vertical and lateral stresses equal to $\sigma_{11} = 75$ kPa and $\sigma_{22} = 30$ kPa, respectively. The values of the above parameters have been selected to represent approximately the loading process occurring within the band, with reference to the dense sand reported in the detail of Fig. 7a ($p_0 = 30$ kPa). The response obtained for σ_{11} constant (and equal to 75 kPa) is also included (dashed) for comparison.

For the selected ratios between volumetric and shear strain, Fig. 10 shows that the shear strength describes a curve exhibiting an initial peak, followed by a minimum and by a second peak. For $\epsilon_{11}/\epsilon_{12} = 0.57$, the shear stress at the second peak is lower than shear stress at the first, but the opposite occurs in the other two cases, for $\epsilon_{11}/\epsilon_{12} = 0.48$ and 0.38 . In the first case, saturation does not occur (as in Fig. 7, for $p_0 = 30, 50, 100$ kPa), but it does occur in the latter cases (as in Fig. 7, for $p_0 = 20$ kPa).

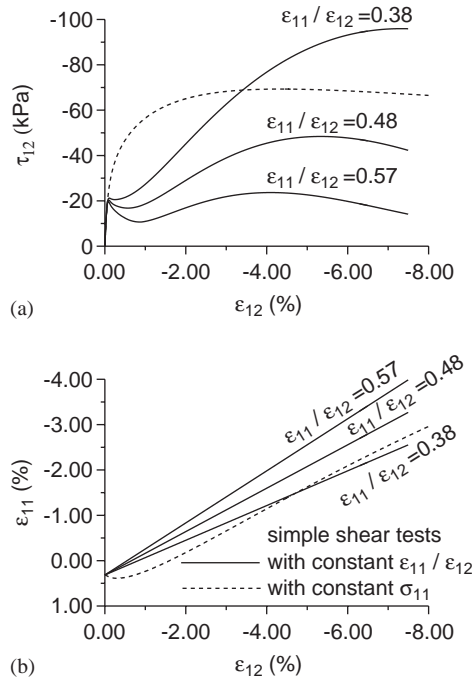


Fig. 10. Response to simple shear, for different fixed deformation ratios $\epsilon_{11}/\epsilon_{12}$. (a) shear stress versus strain, (b) vertical strain versus shear strain.

The difference between the cases where $\epsilon_{11}/\epsilon_{12}$ is equal to 0.48 and 0.38 is that in the latter case the stress oscillation due to band saturation is more serrated. Additional calculations not reported here show that an appropriate ratio of volumetric strain to shear strain in the simple shear test would lead to a situation similar to that reported in Fig. 10 even with an associated flow rule. Therefore, band saturation seems, at least in principle, not to be a result of flow rule non-associativity. However, the dilation rate needed to produce the band saturation would be much larger for associativity than for non-associativity and such a large rate of dilation does not usually exist inside a shear band.

In summary, band saturation in loose sand results from strain hardening occurring inside the band, induced by the contractive behaviour of the material. On the other hand, band saturation in dense sand is forced from kinematic compatibility, constraining the dilation rate.

When band saturation occurs, size effects become particularly important. These effects are explained in Fig. 11, where results for a loose sand have been reported ($e_0 = 0.914$, $p_0 = 100$ kPa) for different ratios $s/h = \{1/1000, 1/200, 1/100, 1/58\}$ between band thickness and sample height. It may be interesting perhaps to note that the depth of the trough of post-peak softening seems to be rather independent of band thickness—so the fact of saturation is not affected and the consequence of having an infinitesimal band

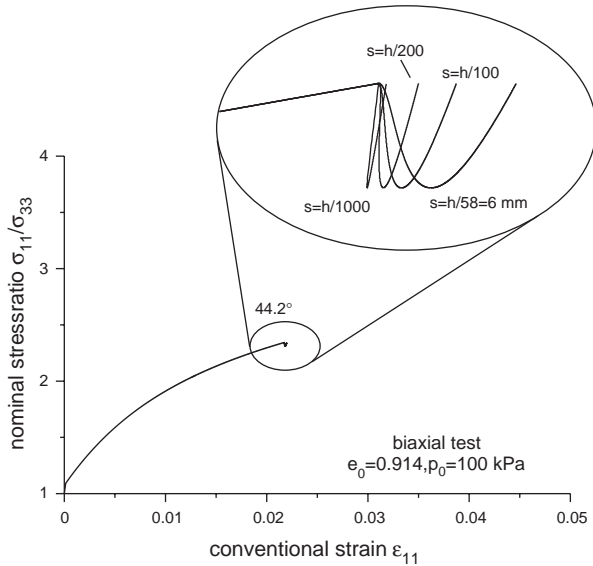


Fig. 11. Simulation of the ‘global’ response of a 350 mm high sample of loose sand showing band saturation for different band thicknesses. (a) nominal axial stress versus conventional strain, (b) conventional volumetric versus axial strain.

is just that the strain required to reach the next peak is correspondingly much smaller. Since the minimum band thickness is presumed to be dictated by the microstructure of the material, for sufficiently high specimens, the ratio becomes, in a sense, a free parameter. When a single band mechanism occurs, heuristic stability requirements lead to the conclusion that the sample will follow the path corresponding to the steepest descent (limited by the elastic unloading stiffness), thus producing snap-back in an appropriate size range. Now the band saturation mechanism changes this conclusion. In fact, since the load increases after a decrease during band saturation, the thickness of the band becomes strongly dependent on the selected stability criterion and this may be much more complicated than the steepest descent criterion adopted by us for simplicity.

To close this section, we presume that our detected band saturation could presage a post-critical behaviour in which many shear bands successively follow each other. To investigate this possibility, we need to define a way to analyse deformation in a post-band saturation regime.

3.4. Post band saturation analysis

The analysis of the post band saturation regime has been performed in a similar way to post-localisation analysis. In particular, we assume at saturation the formation of a new band (outside the saturated band) and the consequent existence of three distinct homogeneous solutions: one outside the bands (ϵ_0), another inside the saturated band

($\mathbf{\epsilon}_s$), and finally one inside the band just formed ($\mathbf{\epsilon}_i$). The second band is taken parallel to the first, since it occurs in a material which is in the same condition for which the first band occurred. Therefore, the deformation rates satisfy the following constraints

$$\dot{\mathbf{\epsilon}}_s = \dot{\mathbf{\epsilon}}_o + \frac{1}{2}[\mathbf{g}_s \otimes \mathbf{n} + \mathbf{n} \otimes \mathbf{g}_s], \quad \dot{\mathbf{\epsilon}}_i = \dot{\mathbf{\epsilon}}_o + \frac{1}{2}[\mathbf{g}_i \otimes \mathbf{n} + \mathbf{n} \otimes \mathbf{g}_i], \tag{54}$$

where \mathbf{g}_i and \mathbf{g}_s are the deformation mode vectors. We denote here with the indices s , i and o the quantities defined inside the saturated band, inside the new band and outside the bands, respectively.

Given that the material inside each band (i.e. the saturated band and the band just formed) and outside the bands undergoes either elastic unloading or plastic loading, eight different cases may exist. As a result of the incremental piecewise linearity of the constitutive relationship, the stress compatibility condition in the case, for example, of plastic loading inside the new band and elastic unloading elsewhere can be written as follows:

$$\mathbf{A}_i^{ep}(\mathbf{n})\mathbf{g}_i = \mathbb{E}_o[\dot{\mathbf{\epsilon}}_o]\mathbf{n} - \mathbb{C}_i[\dot{\mathbf{\epsilon}}_o]\mathbf{n}, \quad \text{and} \quad \mathbf{A}_s^e(\mathbf{n})\mathbf{g}_s = \mathbb{E}_o[\dot{\mathbf{\epsilon}}_o]\mathbf{n} - \mathbb{E}_s[\dot{\mathbf{\epsilon}}_o]\mathbf{n}, \tag{55}$$

and all the other possibilities of loading/unloading can be easily written down. Conditions (55) ensure stress compatibility at both the interfaces between the material outside the bands and the materials inside the new and the saturated bands. Consequently, in the special case in which the saturated and new band are adjacent, stress compatibility at the interface between them is automatically fulfilled.

If the mechanism of band saturation continues forming more than one saturated band and limiting the analysis to the initiation of the process, when only a few bands saturate, each new band behaves with a good approximation in the same way as previously analysed. Therefore, all the saturated bands are made up of the same material which suffered the same deformation history.

When there are n saturated bands and a new one has just formed, Eqs. (54) and (55) still hold true. Moreover, the global kinematic condition expressing the fact that the deformation of the sample may be written as the sum of the contributions inside all the bands plus that outside them is

$$L_o \dot{\mathbf{\epsilon}}_{11}^o + s_o \mathbf{g}_i \cdot \mathbf{e}_1 + n s_o \mathbf{g}_s \cdot \mathbf{e}_1 = \dot{u}_1. \tag{56}$$

In this way, the stress compatibility, Eq. (55), conditions and the kinematic condition at the boundary, Eq. (56), enable the evaluation of the deformation mode vectors \mathbf{g}_i and \mathbf{g}_s .

During the process of band saturation, the continuously forming shear bands progressively transform the original material into a new one, as the result of the plastic strains occurring inside each band: in loose sand the transformed material will be densified, whereas in dense sand it will be loosened. This process will be described as ‘band broadening’, which does not necessarily mean that the subsequent bands form adjacent to each other.

During band broadening, the nominal stress describes a series of small oscillations resulting in the formation of horizontal ‘ripples’ in the stress–strain curve, a phenomenon sharing similarities with stress serrations observed in metal plasticity (Shaw and Kyriakides, 1997). In principle, the process of band broadening may continue indefinitely, although we have restricted the analysis to the early stage of the process.

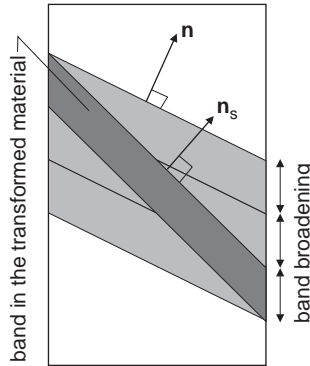


Fig. 12. Sketch of formation of a differently inclined band, within the material transformed by previous.

After a finite-width zone of material exists transformed by the subsequent formation and saturation of adjacent bands, it is possible that a new shear band can initiate within the transformed material. When this occurs it usually terminates the mechanism of subsequent band saturation in dense sand. This possibility will be taken into account by considering that, when subjected to plastic loading again, the transformed material lies outside the elliptic domain (i.e. the hardening modulus is smaller than the critical hardening modulus) and a new shear band can immediately initiate.⁴ In this case, with reference to the situation sketched in Fig. 12, the increments of strains satisfy

$$\dot{\epsilon}_s = \dot{\epsilon}_o + \frac{1}{2} [\mathbf{g}_s \otimes \mathbf{n} + \mathbf{n} \otimes \mathbf{g}_s], \quad \dot{\epsilon}_i = \dot{\epsilon}_s + \frac{1}{2} [\mathbf{g}_i \otimes \mathbf{n}_s + \mathbf{n}_s \otimes \mathbf{g}_i], \quad (57)$$

where \mathbf{n}_s is the normal to the new band which initiates inside the transformed material, belonging to a zone bounded by planes of normal \mathbf{n} . Referring to the conditions of plastic loading inside the band in the transformed material and elastic unloading elsewhere, stress compatibility can be written as follows

$$\mathbf{A}_i^{ep}(\mathbf{n}_s)\mathbf{g}_i = \mathbb{E}_s[\dot{\epsilon}_s]\mathbf{n}_s - \mathbb{C}_i[\dot{\epsilon}_s]\mathbf{n}_s \quad \text{and} \quad \mathbf{A}_s^c(\mathbf{n})\mathbf{g}_s = \mathbb{E}_o[\dot{\epsilon}_o]\mathbf{n} - \mathbb{E}_s[\dot{\epsilon}_o]\mathbf{n}. \quad (58)$$

The global kinematic constraint for the entire specimen is once more given by Eq. (56).

As a result, when a band saturates, two different deformation mechanisms may occur:

- (a) a new band may initiate outside the material transformed by the previously saturated band;
- (b) a new band may initiate within the material transformed by the previously saturated, adjacent bands, with any inclination \mathbf{n}_s (compatible with the thickness of the zone made up of saturated bands and when the hardening modulus of the material is inferior than the critical, Eq. (45)).

⁴ When the hardening modulus falls below the critical value for the onset of strain localisation, localisation with elastic unloading outside the band becomes possible for a finite fan of inclinations (Bigoni and Zaccaria, 1993).

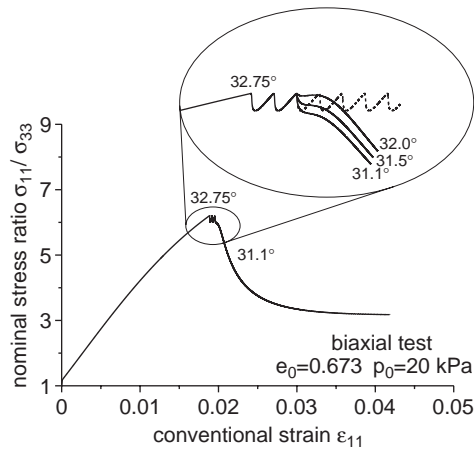


Fig. 13. Post-saturation behaviour for dense sand at low confining pressure. Effects of different band inclinations within the transformed material is detailed.

The choice between the different, possible deformation mechanisms is again based on the heuristic criterion adopted here, namely, the deformation mechanisms leading to the steepest descent in the conventional stress–strain curve has been preferred. For a new band initiating within the transformed material, the steepest descent was found always to be associated with the most steeply inclined (in other words, ‘most nearly vertical’) bands.

Post-saturation behaviour is shown in Fig. 13 for dense sand ($e_0 = 0.673$) at low confining pressure ($p_0 = 20$ kPa), where different possibilities of post-critical behaviour are also indicated in the magnification of the peak of the stress–strain relationship. The process of band broadening is very short: after the saturation of 2 adjacent bands (having an inclination of 32.75°), a new, steeper band is able to initiate inside the transformed material, with an inclination to the vertical of 31.1° (the maximum inclination permitted by the thickness of the transformed material as compared to the specimen width). The band which forms at the end of the band broadening does not saturate and leads to a significant softening. The detail in Fig. 13 shows that steeper bands lead to a steeper descent in the conventional stress–strain response.

The band broadening concept combined with the associated formation of a new, sharp band with a different inclination permits the development of a deformation mechanism yielding a rotation of the band and thus overcoming the kinematic incompatibility that has led to band saturation in dense sand. This explains why *band saturation in dense sand, if and when it occurs, is not persistent*.

In loose sand, band saturation becomes persistent, as can be observed from Fig. 14, for $e_0 = 0.914$ and $p_0 = 100$ kPa. Here the new band (inclined at 42.0°) occurring inside the transformed material (after two bands inclined at 44.21° have formed), also saturates.

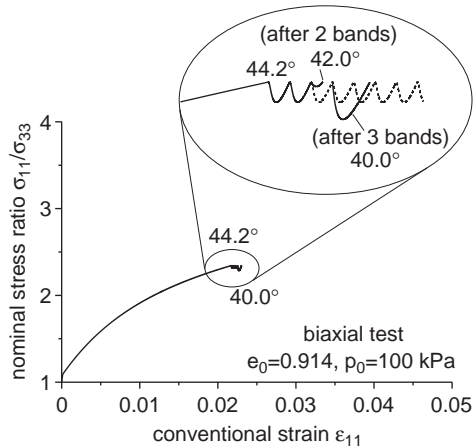


Fig. 14. Post-saturation behaviour for loose sand. Effects of different band inclinations within the transformed material is detailed.

Note that if more bands (for instance 3, as shown in the detail of Fig. 14) are allowed to form and saturate before shear banding in the transformed material occurs, a deeper trough occurs, but saturation mechanism persists.

The fact that the new bands forming inside the transformed material also saturate is consistent with the different nature of band saturation mechanisms in loose and dense sands and with the fact that a process of densification and consequently of strengthening is associated with band saturation only in loose sands.

The experimental evidence of band broadening is missing in dense sand. This is probably connected to the fact that band broadening is expected to occur at negligible confining pressures (which are not usually studied experimentally), to be delayed by the out-of-plane stiffness (Gajo et al., 2004), and finally to have a short life, being replaced very soon by a more inclined sharp band. On the other hand, for loose sands, where the process of band broadening is persistent, there is some experimental evidence obtained by measuring the inhomogeneity of local strain in biaxial tests performed on loose sand by Finno et al. (1997), see their Fig. 9 and, independently, by Chambon and Desrues (1986) using stereophotogrammetric techniques.

Experimental results of biaxial tests on loose ($e_0=0.88-0.90$) Hostun sand, performed at $p_0 = \{100, 200, 400, 800\}$ kPa, are reported in Fig. 15 (taken from Desrues and Hammad, 1989), where shear band inclinations ranging between 27.5° and 33° were found. These shear band measurements are believed to be less accurate than those performed by Finno et al. (1997) and Chambon and Desrues (1986), but the global stress/strain curves are thought to be representative. Therefore, the curves reported in Fig. 15 can be compared with model predictions reported in Fig. 16, where the same values of confining pressures have been considered for loose sand $e_0 = 0.914$.

The satisfactory qualitative agreement between Figs. 15 and 16 supports the key conclusion that the persistent band saturation gives rise to a plateau in the global

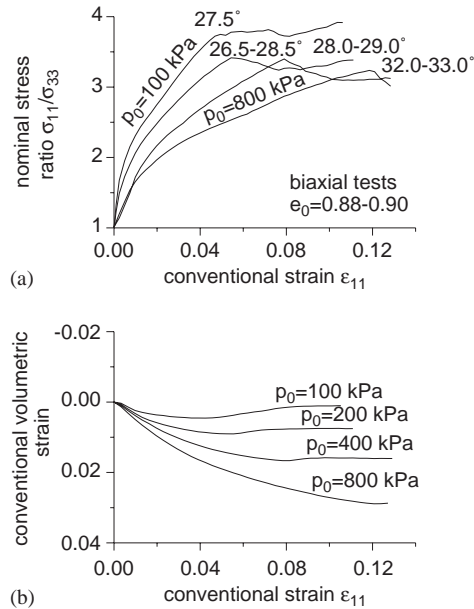


Fig. 15. Experimental results of biaxial tests on loose sand at different confining pressure (taken from Desrues and Hammad, 1989). (a) nominal axial stress versus conventional strain, (b) conventional volumetric versus axial strain.

stress/strain behaviour. However, we observe that the simulated band is much steeper than that measured, a circumstance already discussed for dense sand at low confining pressure. Whether this might be related to the fact that only the *final, steepest* bands have been experimentally detected or it is an inconsistent prediction of our model remains an open problem.

4. Conclusions

Small strain constitutive modelling of strain localisation and post-critical regimes has been described here for granular material, with particular reference to sand. However, several considerations remain valid in the broader context of quasi-brittle materials (including rocks, soils, concrete and other materials).

Although this general subject has been the focus of intensive research in the last thirty years, several new results have been obtained, some of them in a sense expected, others rather surprising. In particular, we have provided a new elastoplastic constitutive framework, specifically tailored for the analysis of strain localisation in sand. Constitutive features such as nonassociativity, shape of yield function, and hardening rule have been confirmed to be important in the definition of the onset of strain localisation.

It has been shown that special roles were played by the induced elastic anisotropy and by the state parameter selected to describe the density and mean-pressure dependency

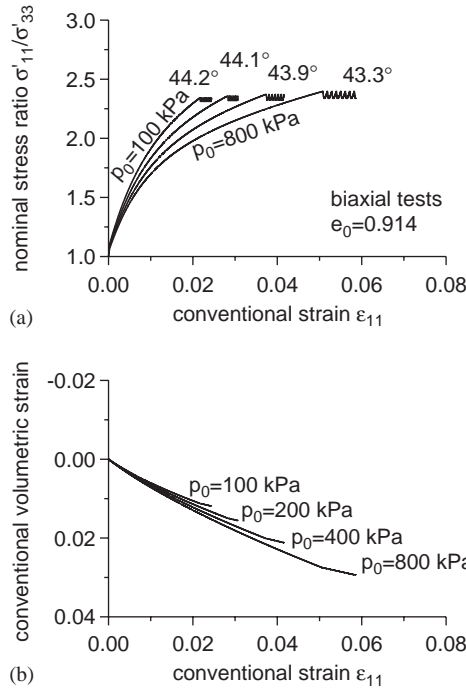


Fig. 16. Simulations showing band broadening in loose sand at different confining pressures. (a) nominal axial stress versus conventional strain, (b) conventional volumetric versus axial strain.

of granular materials. The latter parameter becomes crucial in the post-critical range to describe the density evolution within the localised band.

In order to test the performance of the model beyond the onset of strain localisation, simple analyses, based on assumptions deduced from experimental results, have been preferred to a standard, finite element approach. From the simulations of biaxial compression tests, the following features have been shown:

- occurrence of strain localisation during hardening and related decrease of peak load of the nominal stress/conventional strain curve;
- softening induced by localisation;
- size effects;
- snap-back related to specimen size;
- qualitative and *quantitative* agreement with experimental results.

Some of the above features are well-known. In addition, an unexpected effect was also found, related to the so-called ‘band saturation’. Roughly speaking, in loose sand or in dense sand at low confining pressure, a shear band may ‘close’ soon after formation. The conditions for the formation of a new shear band are then observed to be satisfied in the material outside the band, so that, at band saturation, the material inside

the band elastically unloads, while the material outside plastically reloads resulting in critical conditions and the formation of a second band. A crucial part of the present analysis of the post-saturation behaviour has been to discover whether saturation represents a ‘spurious’ numerical effect or whether it in fact presages a special kind of material instability. The simplicity of the approach adopted for the numerical treatment of the problem, has been advantageous in understanding the material response. The post-saturation analysis indicates a mechanism of ‘shear band accumulation’, producing a zone of plastically transformed material in which, eventually, a new shear band (with different inclination) forms, bringing the previous mechanism of deformation to an end, and leading to a dramatic softening of the nominal stress–strain response.

The extent of the accumulation mechanism crucially depends on confining pressure and material density, so that in a dense sand at small confining pressure, the accumulation is so brief that it is hardly visible. On the other hand, in loose sand the mechanism may become persistent, so that the softening range is avoided and the overall behaviour resembles perfect plasticity. The unusual form of material instability indicated in the present study shares definite similarities with certain phase transformation mechanisms in metals. Although confirmed by a few experiments, we believe that further investigation would be valuable to understand a mechanism which could explain unexpected and sometimes perplexing aspects of the mechanical behaviour of granular materials.

Acknowledgements

We would like to thank Prof. J. Desrues (Institut de Mécanique de Grenoble) for valuable discussions and for having made experimental data available to us. Financial support of the University of Trento and of MIUR-COFIN 2003 “Fenomeni di degrado meccanico di interfacce in sistemi strutturali: applicazioni in Ingegneria Civile ed e campi di ricerca emergenti” (AG and DB), of the UK Engineering and Physical Sciences Research Council (AG and DMW) and of the University of Bristol (DMW) is gratefully acknowledged.

Appendix A. Fourth-order tensor $\partial B/\partial \boldsymbol{\varepsilon}^p$

The following relationships can be easily obtained

$$\frac{\partial(\text{dev } \boldsymbol{\varepsilon}^p)}{\partial \boldsymbol{\varepsilon}^p} = \mathbf{I} \otimes \mathbf{I} - \frac{1}{3} \mathbf{I} \otimes \mathbf{I}, \quad (\text{A.1})$$

$$\frac{\partial \theta_{(\boldsymbol{\varepsilon}^p)}}{\partial \boldsymbol{\varepsilon}^p} = -\frac{\sqrt{3} \text{dev}(\text{dev } \boldsymbol{\varepsilon}^p)^2}{2J_{2(\boldsymbol{\varepsilon}^p)}^{3/2} \sin 3\theta_{(\boldsymbol{\varepsilon}^p)}} + \frac{\text{dev } \boldsymbol{\varepsilon}^p}{2J_{2(\boldsymbol{\varepsilon}^p)} \tan 3\theta_{(\boldsymbol{\varepsilon}^p)}}, \quad (\text{A.2})$$

$$\frac{\partial g(\theta_{(\boldsymbol{\varepsilon}^p)})}{\partial \theta_{(\boldsymbol{\varepsilon}^p)}} = \frac{3(1 - m_\varepsilon)g^2(\theta_{(\boldsymbol{\varepsilon}^p)}) \sin 3\theta_{(\boldsymbol{\varepsilon}^p)}}{2m_\varepsilon}, \quad (\text{A.3})$$

so that, using the chain rule, we get

$$\begin{aligned} \frac{\partial \mathbf{B}}{\partial \boldsymbol{\varepsilon}^p} = & -\beta \left[\mathbf{I} \otimes \mathbf{I} - \frac{1}{3} \mathbf{I} \otimes \mathbf{I} \right] - \frac{\beta^2}{\sqrt{3(3 - 2\beta^2 J_{2(\varepsilon^p)})}} \mathbf{I} \otimes \text{dev } \boldsymbol{\varepsilon}^p \\ & - \left(\text{dev } \boldsymbol{\varepsilon}^p + \frac{2\beta J_{2(\varepsilon^p)}}{\sqrt{3(3 - 2\beta^2 J_{2(\varepsilon^p)})}} \mathbf{I} \right) \otimes \frac{\partial \beta}{\partial \boldsymbol{\varepsilon}^p}, \end{aligned} \tag{A.4}$$

where

$$\frac{\partial \beta}{\partial \boldsymbol{\varepsilon}^p} = \frac{\beta^2}{A_\varepsilon g(\theta_{(\varepsilon^p)})} \left[-\frac{\text{dev } \boldsymbol{\varepsilon}^p}{\sqrt{2J_{2(\varepsilon^p)}}} + \frac{3(1 - m_\varepsilon)g(\theta_{(\varepsilon^p)})\sqrt{J_{2(\varepsilon^p)}} \sin 3\theta_{(\varepsilon^p)}}{\sqrt{2}m_\varepsilon} \frac{\partial \theta_{(\varepsilon^p)}}{\partial \boldsymbol{\varepsilon}^p} \right]. \tag{A.5}$$

It is worth observing that for $\text{dev } \boldsymbol{\varepsilon}^p = \mathbf{0}$, the derivative $\partial \mathbf{B} / \partial \boldsymbol{\varepsilon}^p$ reduces to

$$\frac{\partial \mathbf{B}}{\partial \boldsymbol{\varepsilon}^p} = -\beta \left[\mathbf{I} \otimes \mathbf{I} - \frac{1}{3} \mathbf{I} \otimes \mathbf{I} \right]. \tag{A.6}$$

Appendix B. A bound for positive definiteness of \mathbb{G}

A restriction to the material parameters implying positive definiteness of \mathbb{G} is obtained here. Let us define the following norm of a generic fourth-order tensor \mathbb{A} :

$$\|\mathbb{A}\| = \sqrt{\mathbb{A}_{ijkl} \mathbb{A}_{ijkl}} = \sqrt{\mathbb{A} \cdot \mathbb{A}}, \tag{B.1}$$

where indices are summed between 1 and 3. The fact that Eq. (B.1) defines a norm may be not trivial, therefore, let us show three essential properties. First, the Cauchy–Schwarz inequality can be obtained as follows:

$$\forall \lambda \in \mathfrak{R}, \quad \|\lambda \mathbb{A} + \mathbb{B}\|^2 \geq 0 \Rightarrow |\mathbb{A} \cdot \mathbb{B}| \leq \|\mathbb{A}\| \|\mathbb{B}\|. \tag{B.2}$$

Second, from the Cauchy–Schwarz inequality, the triangle inequality

$$\|\mathbb{A} + \mathbb{B}\| \leq \|\mathbb{A}\| + \|\mathbb{B}\|, \tag{B.3}$$

immediately follows. Recalling now the product between two fourth-order tensors, Eq. (5), we note that

$$\|\mathbb{A} \mathbb{B}\|^2 = \sum_{ijkl} \left(\sum_{st} \mathbb{A}_{ijst} \mathbb{B}_{sthk} \right)^2, \tag{B.4}$$

where we use the summation symbol to help understanding. Now, the Cauchy–Schwarz inequality relative to the second-order tensors which may be associated to the above fourth-order tensors taken at indices ij and hk fixed gives

$$\left(\sum_{st} \mathbb{A}_{ijst} \mathbb{B}_{sthk} \right)^2 \leq \sum_{st} (\mathbb{A}_{ijst})^2 \sum_{pq} (\mathbb{B}_{pqhk})^2. \tag{B.5}$$

Third, using now Eq. (B.5) we obtain

$$\|\mathbb{A}\mathbb{B}\|^2 = \sum_{ijkl} \sum_{st} \mathbb{A}_{ijst} \mathbb{B}_{sthk} \leq \sum_{ijkl} \sum_{st} (\mathbb{A}_{ijst})^2 \sum_{pq} (\mathbb{B}_{pqhk})^2 = \|\mathbb{A}\|^2 \|\mathbb{B}\|^2, \tag{B.6}$$

from which one finally gets

$$\|\mathbb{A}\mathbb{B}\| \leq \|\mathbb{A}\| \|\mathbb{B}\|. \tag{B.7}$$

Application of definition (B.1) gives

$$\|\mathbf{A} \otimes \mathbf{B}\| = \|\mathbf{A}\| \|\mathbf{B}\|, \tag{B.8}$$

whereas, using both definition (B.1) and the triangular inequality yields

$$\|\mathbf{A} \underline{\otimes} \mathbf{B}\| \leq \sqrt{(A_{ih}B_{jk})(A_{ih}B_{jk})},$$

so that

$$\|\mathbf{A} \underline{\otimes} \mathbf{B}\| \leq \|\mathbf{A}\| \|\mathbf{B}\|. \tag{B.9}$$

The positive definiteness of \mathbb{G} is

$$\mathbf{X} \cdot \mathbb{K} \frac{\partial \mathbf{B}}{\partial \mathbf{e}^p} [\mathbf{X}] < \mathbf{X} \cdot \mathbf{X}, \tag{B.10}$$

(for all symmetric second-order tensors \mathbf{X}) which is verified when the stronger condition holds true

$$\|\mathbb{K}\| \left\| \frac{\partial \mathbf{B}}{\partial \mathbf{e}^p} \right\| < 1. \tag{B.11}$$

Note that inequality (B.11) follows from the consideration that for every fourth-order tensor \mathbb{A}

$$\mathbf{X} \cdot \mathbb{A}[\mathbf{X}] = \frac{1}{2} \mathbf{X} \cdot (\mathbb{A} + \mathbb{A}^T)[\mathbf{X}] \leq \frac{1}{2} (\mathbf{X} \cdot \mathbf{X}) \|\mathbb{A} + \mathbb{A}^T\| \leq (\mathbf{X} \cdot \mathbf{X}) \|\mathbb{A}\|.$$

On the other hand, $\|\mathbb{K}\|$ may be easily bounded using Eq. (B.8) as

$$\|\mathbb{K}\| \leq \frac{4\lambda + 2\mu}{\mu(3\lambda + 2\mu)} \|\mathbf{B}^{-1}\|^3 \|\boldsymbol{\sigma}\|, \tag{B.12}$$

so that from Eq. (B.11) we conclude that a bound to positive definiteness of \mathbb{G} is

$$\frac{\|\boldsymbol{\sigma}\|}{2\mu} < \frac{3\lambda + 2\mu}{4(2\lambda + \mu)} \|\mathbf{B}^{-1}\|^{-3} \left\| \frac{\partial \mathbf{B}}{\partial \mathbf{e}^p} \right\|^{-1}. \tag{B.13}$$

Eq. (B.13) makes explicit the fact that positive definiteness of \mathbb{G} poses a restriction on the modulus of the stress (normalised with respect to 2μ), which must be inferior than a function of the constitutive parameters and of the plastic strain. Therefore, for ‘stiff’ materials such as concrete or rock, Eq. (B.13) tends to be automatically satisfied, since $\|\boldsymbol{\sigma}\|/\mu$ takes small values. However, this may be not the case of loose sand. Expanding on this point, we use the expression for $\partial \mathbf{B}/\partial \mathbf{e}^p$ obtained in Appendix A, Eq. (A.4),

thus obtaining

$$\begin{aligned} \left\| \frac{\partial \mathbf{B}}{\partial \boldsymbol{\varepsilon}^p} \right\| &\leq \beta \left(1 + \frac{1}{\sqrt{2}} \right) + \frac{\beta^2 \sqrt{2J_{2(\varepsilon^p)}}}{\sqrt{3 - 2\beta^2 J_{2(\varepsilon^p)}}} \\ &+ \left(\sqrt{2J_{2(\varepsilon^p)}} + \frac{2\beta J_{2(\varepsilon^p)}}{\sqrt{3 - 2\beta^2 J_{2(\varepsilon^p)}}} \right) \left\| \frac{\partial \beta}{\partial \boldsymbol{\varepsilon}^p} \right\|, \end{aligned} \tag{B.14}$$

where

$$\left\| \frac{\partial \beta}{\partial \boldsymbol{\varepsilon}^p} \right\| \leq \frac{\beta^2}{A_\varepsilon g(\theta_{(\varepsilon^p)})} \left[1 + \frac{3(1 - m_\varepsilon)g(\theta_{(\varepsilon^p)})\sqrt{J_{2(\varepsilon^p)}} \sin 3\theta_{(\varepsilon^p)}}{\sqrt{2}m_\varepsilon} \left\| \frac{\partial \theta_{(\varepsilon^p)}}{\partial \boldsymbol{\varepsilon}^p} \right\| \right], \tag{B.15}$$

and

$$\left\| \frac{\partial \theta_{(\varepsilon^p)}}{\partial \boldsymbol{\varepsilon}^p} \right\| = \frac{\sqrt{3} \|\text{dev}(\text{dev } \boldsymbol{\varepsilon}^p)^2\|}{2J_{2(\varepsilon^p)}^{3/2} \sin 3\theta_{(\varepsilon^p)}} + \frac{|\cot 3\theta_{(\varepsilon^p)}|}{\sqrt{2}J_{2(\varepsilon^p)}}. \tag{B.16}$$

Expression (42) of \mathbf{B}^{-1} and Eqs. (B.14)–(B.16) indicate the contribution that the constitutive parameters play in the positive definiteness of \mathbb{G} .

We note that the bound (B.13) to the positive definiteness of \mathbb{G} is not very strict since, assuming null elastic anisotropy (i.e. $\boldsymbol{\varepsilon}^p = \mathbf{0}$ and $\beta = A_\varepsilon/B_\varepsilon$) and isotropic stress ($\boldsymbol{\sigma} = -p\mathbf{1}$), Eq. (B.13) gives

$$\frac{p}{2\mu} < \frac{\sqrt{2}}{9(1 + \sqrt{2})} \frac{B_\varepsilon}{A_\varepsilon} \frac{3\lambda + 2\mu}{4(2\lambda + \mu)}, \tag{B.17}$$

whereas the exact value for positive definiteness of \mathbb{G} is

$$\frac{p}{2\mu} < \frac{B_\varepsilon}{A_\varepsilon} \frac{3\lambda + 2\mu}{3\lambda + 4\mu}. \tag{B.18}$$

Since μ is comparatively much higher for dense sand than for loose [see Eq. (D.1)], we conclude that (B.13) provides a useful bound for dense sand, but may not be particularly accurate for loose sand.

Appendix C. Condition for the positive definiteness of the fabric tensor \mathbf{B}

We begin by noting that for all non-null vectors \mathbf{x}

$$\mathbf{x} \cdot \mathbf{B} \mathbf{x} \geq \left[\sqrt{1 - \frac{1}{3} A_\varepsilon^2 g^2(\theta_{(\varepsilon^p)})} - \frac{A_\varepsilon g(\theta_{(\varepsilon^p)})}{B_\varepsilon g(\theta_{(\varepsilon^p)}) + |\text{dev } \boldsymbol{\varepsilon}^p|} (\text{dev } \boldsymbol{\varepsilon}^p)_{\max} \right] \mathbf{x} \cdot \mathbf{x}, \tag{C.1}$$

where $(\text{dev } \boldsymbol{\varepsilon}^p)_{\max} > 0$ is the maximum eigenvalue of the tensor $\text{dev } \boldsymbol{\varepsilon}^p$. Now, since tensor $\text{dev } \boldsymbol{\varepsilon}^p$ is deviatoric, the intermediate eigenvalue $(\text{dev } \boldsymbol{\varepsilon}^p)_{\text{int}}$ may be obtained through

$$(\text{dev } \boldsymbol{\varepsilon}^p)_{\text{int}} = -(\text{dev } \boldsymbol{\varepsilon}^p)_{\max} - (\text{dev } \boldsymbol{\varepsilon}^p)_{\min}, \tag{C.2}$$

where $(\text{dev } \varepsilon^p)_{\min} < 0$ is the minimum eigenvalue of $\text{dev } \varepsilon^p$. Introducing now $\rho = (\text{dev } \varepsilon^p)_{\min}/(\text{dev } \varepsilon^p)_{\max}$, we get

$$\mathbf{x} \cdot \mathbf{B}\mathbf{x} \geq \left[\sqrt{1 - \frac{1}{3} A_\varepsilon^2 g^2(\theta_{(\varepsilon^p)})} - \frac{(\text{dev } \varepsilon^p)_{\max} A_\varepsilon g(\theta_{(\varepsilon^p)})}{B_\varepsilon g(\theta_{(\varepsilon^p)}) + (\text{dev } \varepsilon^p)_{\max} \sqrt{2} \sqrt{1 + \rho + \rho^2}} \right] \mathbf{x} \cdot \mathbf{x}, \tag{C.3}$$

from which we obtain

$$\mathbf{x} \cdot \mathbf{B}\mathbf{x} \geq \left[\sqrt{1 - \frac{1}{3} A_\varepsilon^2 g^2(\theta_{(\varepsilon^p)})} - \frac{A_\varepsilon g(\theta_{(\varepsilon^p)})}{\sqrt{2} \sqrt{1 + \rho + \rho^2}} \right] \mathbf{x} \cdot \mathbf{x}. \tag{C.4}$$

Eq. (C.4) implies that when condition (43) is satisfied, tensor \mathbf{B} is positive definite. Note that

$$1 \leq \frac{1}{\sqrt{\frac{1}{3} + \frac{1}{2(1+\rho+\rho^2)}}} \leq \sqrt{2}, \tag{C.5}$$

so that, when $g(\theta_{(\varepsilon^p)})A_\varepsilon \leq 1$, Eq. (43) is automatically satisfied.

Appendix D. Model calibration and simulations of the homogeneous response

The constitutive framework that has been presented is tailored to describe the mechanical behaviour of sand under monotonic loading and in a range of mean pressure sufficiently low to avoid grain crushing. The model is defined by 14 parameters, five of which defining the elastic behaviour (λ and μ , A_ε , B_ε , m_ε) and the remaining nine describing the plastic behaviour (v_A , A , ϕ_{cv} , m , k , A , k_d , B , R).

The constants λ and μ can be deduced from the fact that the shear modulus μ_0 obtained from the velocity of propagation of elastic waves is well described by the empirical relationship proposed by [Hardin and Black \(1968\)](#)

$$\mu_0 = 3230 \frac{(3.97 - v)^2}{v} \sqrt{p}, \tag{D.1}$$

(where both μ_0 and p are expressed in kPa) so that it depends on specific volume v and mean pressure p . Eq. (D.1) describes the very high stiffness that granular media exhibit when subjected to very small strain increments. Here it becomes reasonable to assume that the effective value of elastic shear modulus is a fraction of μ_0 , in particular, $\mu = \mu_0/5$. Moreover, we drop the dependence of μ_0 on p and v by referring to average values relative to the different testing conditions that will be analysed. Once μ has been fixed, constant λ is obtained assuming a Poisson’s ratio equal to 0.1, a value that was already employed by [Gajo and Muir Wood \(1999a\)](#).

In order to provide the data needed to calibrate the three constitutive parameters describing the evolution of elastic anisotropy, we have used the experimental method proposed and described by [Gajo et al. \(2001\)](#) and [Gajo \(2004\)](#) for sand tested in a conventional triaxial cell. The method consists in measuring the inclination, denoted

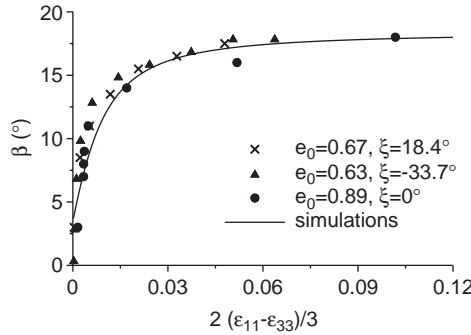


Fig. 17. Simulated and measured evolution of elastic anisotropy along different compression loading paths.

Table 1
Values of soil parameters for describing the behaviour of Hostun sand RF

Parameter	Description	Value
μ	Elastic shear modulus (constant)	$\mu_0/5$
ν	Poisson's ratio	0.1
A_e	Parameter controlling the asymptotic value of elastic anisotropy in uniaxial compression	1.1
B_e	Parameter controlling the hyperbolic evolution of elastic anisotropy with plastic strain	0.02
m_e	Parameter controlling the asymptotic value of elastic anisotropy in uniaxial extension	0.45
v_A	Intercept for critical-state line in $v - \ln p$ plane at $p = 1$ kPa	1.969
A	Slope of critical-state line in $v - \ln p$ plane	0.030
ϕ_{cv}	Critical-state angle of friction	32°
m	Parameter controlling the deviatoric section of the yield surface	0.8
k	Link between changes in state parameter and current size of the yield surface	2.5
A	Dilatancy parameter	0.6
k_d	State parameter contribution in flow rule	2.2
B	Parameter controlling hyperbolic stiffness relationship	0.004
R	Initial size of the yield surface	0.1

by β , of small *undrained* unloading/reloading cycles in the $q - p$ representation usually employed in soil mechanics (q is an invariant of deviatoric stress), superimposed upon a *drained* loading path of given inclination ξ . The above-mentioned experimental results, reported in Fig. 17 together with simulations, allow us now to quantify the way in which our model is able to simulate the induced elastic anisotropy. In the figure, the inclination β is shown as a function of deviatoric strain $2(\epsilon_{11} - \epsilon_{33})/3$, for different values of initial density ($e_0 = \{0.62, 0.89\}$) and drained loading path inclinations ($\xi = \{-33.7^\circ, 0, 18.4^\circ\}$). Note that, since all simulations provide practically coincident results, only one is reported (relative to $\xi = 18.4^\circ$). It can be observed in Fig. 17 that an asymptotic value of elastic anisotropy is obtained at large strains and that the evolution and the asymptotic value of elastic anisotropy are somewhat independent of the initial density and of the loading path.

The parameters describing the inelastic behaviour can be shown to have a clear physical meaning and the interested reader is referred to (Gajo and Muir Wood, 1999a,b)

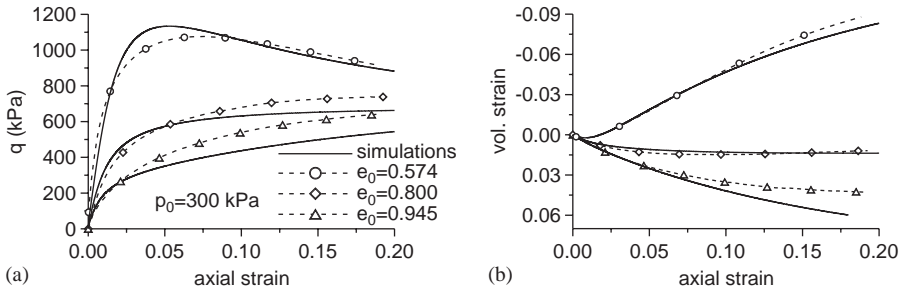


Fig. 18. Comparison between simulations and experiments: effects of the initial density on drained, conventional triaxial compression tests, with the same initial pressure, $p_0 = 300$ kPa, for Hostun sand RF. (a) deviatoric stress q versus axial strain, (b) volumetric versus axial strain.

for a full discussion, relative to Hostun sand RF. The optimal values for the parameters employed here are very similar to those reported by Gajo and Muir Wood (1999a,b). These, together with the parameters describing the elastic behaviour, are listed in Table 1 and remain valid for all simulations presented throughout the paper. A key feature for describing deformation evolution inside the shear band is the ability of the presented model to describe the stress/strain behaviour in a wide range of density for fixed values of material parameters. To appreciate this, we have included in Fig. 18 comparisons of the model response with experimental results referred to triaxial tests. In particular, the deviatoric stress measure q and the volumetric strain are reported in Fig. 18a and b, for a broad interval of density ($e_0 = \{0.574, 0.800, 0.945\}$).

References

- Argyris, J.H., Faust, G., Szimmat, J., Warnke, P., Willam, K., 1974. Recent developments in the finite element analysis of prestressed concrete reactor vessels. *Nucl. Eng. Des.* 28, 42–75.
- Arthur, J.R.F., Dunstan, T., Al-Ani, Q.A.J.L., Assadi, A., 1977. Plastic deformation and failure in granular media. *Géotechnique* 27, 53–74.
- Bardi, F.C., Yun, H.D., Kyriakides, S., 2003. On the axisymmetric progressing crushing of circular tubes under axial compression. *Int. J. Solids Struct.* 40, 3137–3155.
- Been, K., Jefferies, M.G., 1985. A state parameter for sands. *Géotechnique* 35, 99–112.
- Benallal, A., Comi, C., 2003. Perturbation growth and localization in fluid-saturated inelastic porous media under quasi-static loadings. *J. Mech. Phys. Solids* 51, 851–899.
- Bigoni, D., 2000. Bifurcation and instability of nonassociative elasticplastic solids. In: Petryk, H. (Ed.), *CISM Lecture Notes No. 414 “Material Instabilities in Elastic and Plastic Solids”*. Springer-Verlag, Wien, New York, pp. 1–52.
- Bigoni, D., Hueckel, T., 1991. Uniqueness and localization II. Coupled elastoplasticity. *Int. J. Solids Struct.* 28, 215–224.
- Bigoni, D., Loret, B., 1999. Effects of elastic anisotropy on strain localization and flutter instability in plastic solids. *J. Mech. Phys. Solids* 47, 1409–1436.
- Bigoni, D., Zaccaria, D., 1993. On strain localization analysis of elastoplastic materials at finite strains. *Int. J. Plasticity* 9, 21–33.
- Bigoni, D., Loret, B., Radi, E., 2000. Localization of deformation in plane elastic-plastic solids with anisotropic elasticity. *J. Mech. Phys. Solids* 48, 1441–1466.

- Brannon, R.M., Drugan, W.J., 1993. Influence of nonclassical elastic plastic constitutive features on shock-wave existence and spectral solutions. *J. Mech. Phys. Solids* 41, 297–330.
- Capurso, M., 1979. Extremum theorems for the solution of the rate problem in elastic-plastic fracturing structures. *J. Struct. Mech.* 7, 411–434.
- Chambon, R., Desrues, J., 1986. Discussion on comparison of frictional material models with respect to shear band initiation. *Géotechnique* 36, 133–135.
- Collins, I.F., Houlsby, G.T., 1997. Application of thermomechanical principles to the modelling of geotechnical materials. *Proc. R. Soc. Lond.* 453, 1975–2001.
- Dafalias, Y.F., 1977. Il'iusin's postulate and resulting thermodynamic conditions on elastic–plastic coupling. *Int. J. Solids Struct.* 13, 239–251.
- Desrues, J., Hammad, W., 1989. Shear band dependency on mean stress level. In: Dembicki, E., Gudheus, G., Sikora, Z. (Eds.), *Numerical Methods for Localisation and Bifurcation of Granular Materials*. Gdansk, Poland, pp. 57–67.
- Desrues, J., Lanier, J., Stutz, P., 1985. Localisation of the deformation in tests on sand sample. *Engineering Fracture Mechanics* 21, 909–921.
- Desrues, J., Chambon, R., Mokni, M., Mazerolle, F., 1996. Void ratio evolution inside shear bands in triaxial sand specimens studied by computed tomography. *Géotechnique* 46, 529–546.
- Dougill, J.W., 1976. On stable progressively fracturing solids. *Z. Angew. Math. Phys.* 27, 423–437.
- Drescher, A., Vardoulakis, I., Han, C., 1990. A biaxial apparatus for testing soils. *Geotech. Eng. J. ASTM* 13, 226–234.
- Finno, R.J., Harris, W.W., Mooney, M.A., Viggiani, G., 1997. Shear bands in plane strain compression of loose sand. *Géotechnique* 47, 149–165.
- Gajo, A., 2003. Instability phenomena in sand samples. Ph.D. Thesis, University of Bristol, Bristol, UK.
- Gajo, A., 2004. The influence of system compliance on collapse of triaxial sand samples. *Can. Geotech. J.*, 41, 257–273.
- Gajo, A., Muir Wood, D., 1999a. A kinematic hardening constitutive model for sands: the multiaxial formulation. *Int. J. Numer. Anal. Meth. Geomechanics* 23, 925–965.
- Gajo, A., Muir Wood, D., 1999b. Severn-trent sand: a kinematic hardening constitutive model for sands: the q – p formulation. *Géotechnique* 49, 595–614.
- Gajo, A., Bigoni, D., Muir Wood, D., 2001. Stress induced elastic anisotropy and strain localization in sand. In: Mühlhaus, H.B., Dyskin, A., Pasternak, E. (Eds.), *Bifurcation and Localization Theory in Geomechanics*. Swets & Zeitlinger, Lisse, pp. 37–44.
- Gajo, A., Bigoni, D., Muir Wood, D., 2004. Effects of material and testing characteristics on post-critical shear band development. Submitted.
- Hall, E.O., 1970. *Yield Point Phenomena in Metals and Alloys*. Plenum Press, New York.
- Han, C., Drescher, A., 1993. Shear bands in biaxial tests on dry coarse sand. *Soil Found.* 33, 118–132.
- Hardin, B.O., Black, W.L., 1968. Vibration modulus of normally consolidated clay. *J. Soil Mech. Found. Div. ASCE* 94, 353–369.
- Hill, R., 1978. Aspects of invariance in solid mechanics. In: Yih, C.-S. (Ed.), *Advances in Applied Mechanics*, Vol. 18. Academic Press, New York, pp. 1–75.
- Hill, R., Rice, J.R., 1973. Elastic potentials and the structure of inelastic constitutive laws. *SIAM J. Appl. Math.* 25, 448–461.
- Hueckel, T., 1975. On plastic flow of granular and rock-like materials with variable elasticity moduli. *Bull. Pol. Acad. Sci., Ser. Techn.* 23, 405–414.
- Hueckel, T., 1976. Coupling of elastic and plastic deformation of bulk solids. *Meccanica* 11, 227–235.
- Hueckel, T., Maier, G., 1977. Incremental boundary value problems in the presence of coupling of elastic and plastic deformations: a rock mechanics oriented theory. *Int. J. Solids Struct.* 13, 1–15.
- Hutchinson, J.W., Tvergaard, V., 1981. Shear band formation in plane strain. *Int. J. Solids Struct.* 17, 451–470.
- Johan, Z., Hughes, T.J.R., Shakib, F., 1991. A globally convergent matrix-free algorithm for implicit time-marching schemes arising in finite element analysis in fluids. *Comput. Meth. Appl. Mech. Eng.* 87, 281–304.
- Loret, B., Harireche, O., 1991. Acceleration waves, flutter instabilities and stationary discontinuities in inelastic porous media. *J. Mech. Phys. Solids* 39, 569–606.

- Loret, B., Rizzi, E., 1999. Strain localization in fluid-saturated anisotropic elastic-plastic porous media with double porosity. *J. Mech. Phys. Solids* 47, 503–530.
- Maier, G., Hueckel, T., 1979. Nonassociated and coupled flow-rules of elastoplasticity for rock-like materials. *Int. J. Rock Mech. Min. Sci.* 16, 77–92.
- Mathies, H., Strang, G., 1979. The solution of non-linear finite element equations. *Int. J. Numer. Meth. Eng.* 11, 1613–1626.
- Mróz, Z., 1963. Non-associated flow laws in plasticity. *J. de Mécanique* 2, 21–42.
- Mróz, Z., 1966. On forms of constitutive laws for elastic–plastic solids. *Arch. Mech. Stosowanej* 18, 1–34.
- Muir Wood, D., 2002. Some observations of volumetric instabilities in soils. *Int. J. Solids Struct.* 39, 3429–3449.
- Needleman, A., 1988. Material rate dependence and mesh sensitivity in localization problems. *Comput. Meth. Appl. Mech. Eng.* 67, 69–85.
- Papka, S.D., Kyriakides, S., 1999. Biaxial crushing of honeycomb-Part. I: experiments. *Int. J. Solids Struct.* 36, 4367–4396.
- Petryk, H., Thermann, K., 2002. Post-critical plastic deformation in incrementally nonlinear materials. *J. Mech. Phys. Solids* 50, 925–954.
- Rice, J.R., 1975. On the stability of dilatant hardening for saturated rock masses. *J. Geophys. Res.* 80, 1531–1536.
- Rice, J.R., 1977. The localization of plastic deformation. In: Koiter, W.T. (Ed.), *Theoretical and Applied Mechanics*. North-Holland, Amsterdam, pp. 207–220.
- Rice, J.R., Rudnicki, J.W., 1980. A note on some features of the theory of localization of deformation. *Int. J. Solids Struct.* 16, 597–605.
- Roger, W., Desrués, J., Viggiani, G., 1998. Experiments on strain localization in dense sand under isochoric conditions. In: Oka, F. (Ed.), *Localization and Bifurcation Theory for Soils and Rocks*. Balkema, Rotterdam, pp. 239–248.
- Roscoe, K.H., 1970. The influence of strains in soil mechanics. 10th Rankine Lecture. *Géotechnique* 20, 129–170.
- Roscoe, K.H., Arthur, J.R.F., James, R.G., 1963. The determination of strains in soils by an X-ray method. *Civil Eng. Public Works Rev.* 684, 873–876; 685, 1009–1012.
- Rudnicki, J.W., 2001. Diffusive instabilities in dilating and compacting geomaterials. In: Chuang, T.-J., Rudnicki, J.W. (Eds.), *Multiscale Deformation and Fracture in Materials and Structures*. Kluwer, Dordrecht, pp. 159–182.
- Rudnicki, J.W., Rice, J.R., 1975. Conditions for the localization of deformations in pressure-sensitive dilatant materials. *J. Mech. Phys. Solids* 23, 371–394.
- Schaeffer, D.G., 1990. Instability and ill-posedness in the deformation of granular materials. *Int. J. Num. Anal. Meth. Geomech.* 14, 253–278.
- Schaeffer, D.G., Shearer, M., 1997. The influence of material non-uniformity preceding shear band formation in a model for granular flow. *Euro. J. Appl. Math.* 8, 457–483.
- Schofield, A.N., Wroth, C.P., 1968. *Critical State Soil Mechanics*. McGraw-Hill, London.
- Shaw, J.A., Kyriakides, S., 1997. Initiation and propagation of localized deformation in elasto-plastic strips under uniaxial tension. *Int. J. Plasticity* 13, 837–871.
- Shearer, M., Schaeffer, D.G., 1994. Unloading near a shear band in granular material. *Quart. Appl. Math.* 52, 579–600.
- Simo, J., Hughes, T.J.R., 1987. General return mapping algorithms for rate-independent plasticity. In: Desai, C.S. et al. (Eds.), *Constitutive Laws for Engineering Materials: Theory and Applications*. Elsevier Science Publ. Co., pp. 221–231.
- Tatsuoka, F., Nakamura, S., Huang, C.C., Tani, K., 1990. Strength anisotropy and shear band direction in plane strain tests of sand. *Soils Found.* 30, 35–54.
- Tvergaard, V., 1982. Influence of void nucleation on ductile shear fracture at a free surface. *J. Mech. Phys. Solids* 30, 399–425.
- Valanis, K.C., 1990. A theory of damage in brittle materials. *Eng. Fract. Mech.* 36, 403–416.
- Vardoulakis, I., 1978. Equilibrium bifurcation of granular earth bodies. *Advances in analysis of geotechnical instabilities*. SM study 13, Paper 3, 65–119, University of Waterloo Press.

- Vardoulakis, I., 1980. Shear band inclination and shear modulus of sand in biaxial tests. *Int. J. Num. Anal. Meth. Geomech.* 4, 103–119.
- Vardoulakis, I., 1988. Theoretical and experimental bounds for shear-band bifurcation strain in biaxial tests on dry sand. *Res Mech.* 23, 239–259.
- Vardoulakis, I., Graf, B., 1985. Calibration of constitutive models for granular materials using data from biaxial experiments. *Géotechnique* 35, 299–317.
- Wong, T.F., Baud, P., Klein, E., 2001. Localized failure modes in a compactant porous rock. *Geophys. Res. Lett.* 28, 2521–2524.
- Wroth, C.P., Bassett, R.H., 1965. A stress–strain relationship for the shearing behaviour of a sand. *Géotechnique* 15, 32–56.